PURDUE UNIVERSITY
GRADUATE SCHOOL
Thesis/Dissertation Acceptance

This is to certify that the thesis/dissertation prepared

By MARYAM ALIBEIK

Entitled

DIFFERENT CONFIGURATIONS OF MICROGRIDS AND POWER CONVERTERS

For the degree of   Master of Science in Electrical and Computer Engineering

Is approved by the final examining committee:

DR. EUZELI DOS SANTOS

DR. MAHER RIZKALLA

DR. STEVEN ROVNYAK

To the best of my knowledge and as understood by the student in the *Thesis/Dissertation Agreement. Publication Delay, and Certification/Disclaimer (Graduate School Form 32)*, this thesis/dissertation adheres to the provisions of Purdue University's "Policy on Integrity in Research" and the use of copyrighted material.

DR. EUZELI DOS SANTOS

Approved by Major Professor(s): _____

Approved by: DR. BRIAN KING   07/29/2014

Head of the Department Graduate Program   Date

DIFFERENT CONFIGURATIONS OF MICROGRIDS AND POWER

CONVERTERS

A Thesis

Submitted to the Faculty

of

Purdue University

by

Maryam Alibeik

In Partial Fulfillment of the

Requirements for the Degree

of

Master of Science in Electrical and Computer Engineering

August 2014

Purdue University

Indianapolis, Indiana

UMI Number: 1573479

UMI

Dissertation Publishing

UMI 1573479

ProQuest

This work is dedicated to my parents.

ACKNOWLEDGMENTS

I would like to express my deepest appreciation to my advisor Dr. Euzeli dos Santos for his excellent support, guidance, and patience during my Master studies. I am grateful to have such an advisor and looking forward to further working with him in the future.

I also want to thank Dr. Maher Rizkalla and Dr. Steven Rovnyak for accepting being my Committee members.

I have to thank Sherrie Tucker for her great support and guidance in the Department of Electrical and Computer Engineering, who has been always the best person to go to for finding the best solution.

Last but not least, I have to thank my family for their unconditional love and support and specially my sister, Nazanin, who has always been my best friend. I also want to thank Sepehr for his unconditional patience and support both emotionally and in my studies.

TABLE OF CONTENTS

LIST OF TABLES

LIST OF FIGURES

ABSTRACT

Alibeik, Maryam. MSECE, Purdue University, August 2014. Different Configurations of Microgrids and Power Converters. Major Professor: Dr. Euzeli dos Santos Jr.

This thesis proposes a two-phase microgrid system with voltages in quadrature. The two-phase microgrid system presents the following advantages: 1) constant power through the power line at balanced condition; 2) two voltages available by using a three-wire system; 3) optimized voltage utilization compared to a three-phase system; and 4) a direct connection of both symmetrical two-phase and single-phase machines. Power analysis and symmetrical components of this kind of microgrid have also been studied through this thesis. Besides the two-phase microgrid system, the hybrid DC/AC microgrid has been analyzed. Both hybrid DC/AC and two-phase microgrid need power interfaces such as power converters to be connected to the grid. Also two different types of power converters have been proposed and studied during this thesis.

1. INTRODUCTION

1.1   Microgrid

A well-defined traditional power distribution system has a radial topology [1,2] and a single unit of power generation to feed end users. The use of individual distributed generators can cause some problems during the disturbances in a system such as harming the transmission system as well as the system's loads. For avoiding such problems one way is to realize a batch of loads and sources as one controllable system, called as "microgrid" [3–5].

A microgrid can be defined as a localized grouping of electricity generation, energy storage, and loads that normally operate connected to a traditional centralized grid (macrogrid). The multiple dispersed generation sources and the ability to isolate the microgrid from a larger networkwould provide highly reliable electric power. Besides the conventional microgrids with either DC- or AC-links, it is also possible to implement hybrid DC/AC microgrids as considered in [6–8].

Sources used in a microgrid are often small ($< 500kW$) [9]. The main advantages of those solutions are: 1) high reliability [10–12], which can be obtained by using power electronics interfaces together with fast protection systems [9]. In [13] it has been proposed a new method for evaluating the reliability of microgrids including DGs. [14] also conducts several case studies in order to demonstrate impact of CHO-Based DERs on the microgrid reliability, 2) use of renewable energy with zero emissions, allowing plants to be near enough to cities [15], 3) reduction or elimination of the need for central dispatch [16], 4) reduction of the long-distance losses related to transmission lines [17], and 5) improvement of power quality [18].

In the modern scenario, the utility grid is supposed to guarantee load management, demand side management, as well as to use the market price of electricity and

forecasting of energy (e.g., based on wind and solar renewable sources) in order to optimize the whole distribution system [19]. An electric power system requires several goals in its optimized operation, such as high efficiency, high reliability, good quality of service and high level of security [20]. Those objectives can be obtained in the new power distribution systems through advances in control, communication and information technology, as well as extensive use of power electronics. Notice that the power line type is not necessarily defined anymore by a centralized generation unit that delivers the same type of energy to all loads connected to it, as it used to be in the first poly-phase electric power system at Niagara Falls. This arrangement has lasted for more than 100 years. Now the power distribution process goes through electronic devices that allow more flexibility regarding how the electric link is defined. Research effort has been developed towards: 1) DC microgrid link [19], 2) single-phase 60Hz AC microgrid link [20], 3) single-phase high-frequency AC microgrid link [21], 4) three-phase three-wire microgrid link [22], and 5) three-phase four-wire microgrid link [23]. A comparison among three of those microgrids is furnished in [24]. Recently a hybrid AC/DC microgrid has been studied by [25], which presents the main advantage of furnishing both DC and AC voltages throughout the line, avoiding either DC-to-DC or AC-to-DC conversions, thus improving the efficiency of the whole system.

This chapter contributes to the debate of how energy sources with different types of delivered power (DC or AC) and different levels of generated voltage (higher or lower voltage) can impact the decision made regarding the electrical link topology employed to distribute energy as presented in Fig. 1.1.

The electrical power line architectures compared in this paper are: 1) DC; 2) single-phase, which includes standard 60Hz, high-frequency, and single split-phase links; 3) hybrid AC/DC link; 4) symmetrical two-phase with voltages in quadrature; 5) three-phase link with both three and four wires; and finally 6) poly-phase lines (four-, five- and six-phase links). The rationale is that, the microgrid is fed by strong energy sources, such as the wind and solar farms presented in Fig. 1.1, as well as by weak energy sources, i.e., residential PV and wind generation. To guarantee a

fair comparison among the electrical links studied in this section, it will be assumed that all power systems considered in this section will have the same voltage insulation rating with the same power capability.
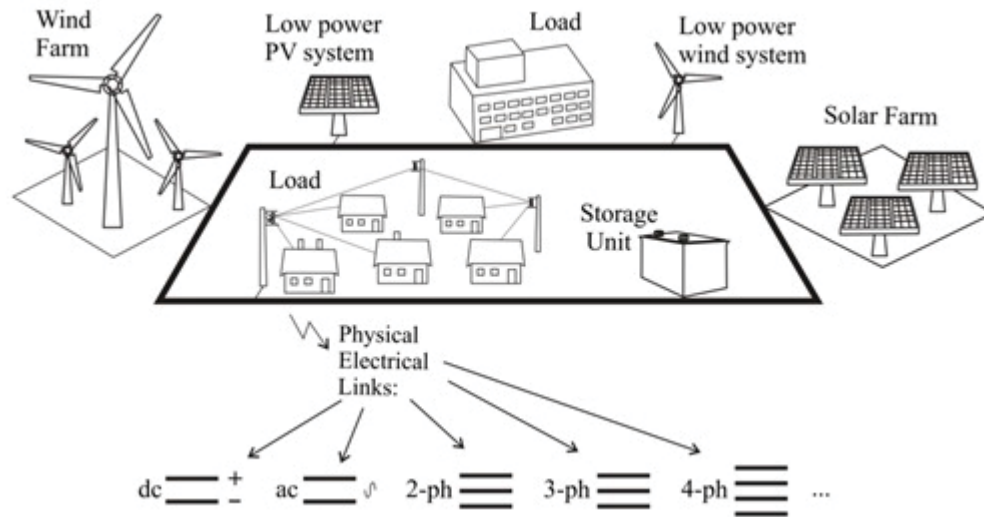
Fig. 1.1. Microgrid environment highlighting the physical electrical link.

1.1.1 DC Microgrid Link

The DC Microgrid uses DC distribution in order to provide the high quality power [26, 27]. In order to minimize the loss and maximize the energy efficiency one could utilize the DG output in DC form. Using the low voltage DC Microgrid may have some advantages over the conventional AC distribution system such as: 1) There only needs to be one DC/AC inverter needed for connecting the mains to the DC grid; 2) When a fault happens in the AC network, the DC grid will operate in stand-alone mode which will keep the loads from being damaged. DC was the earliest form of electrical power [28] and it is a potential candidate to be employed in the power line of the system in Fig. 1.1. It is expected that with DC power available on the electrical link, the ac-to-dc power conversion will be eliminated so that it is possible to save more energy. The total savings could be magnified since DC power is employed largely

on our everyday devices, such as computers, cellphones, TVs, printers, LED lights, etc. The DC microgrid can be beneficial even for AC loads like induction machines, due to the trend of replacement for variable-speed motor drives, especially for higher powers. Fig. 1.2 shows a typical configuration of a DC microgrid.
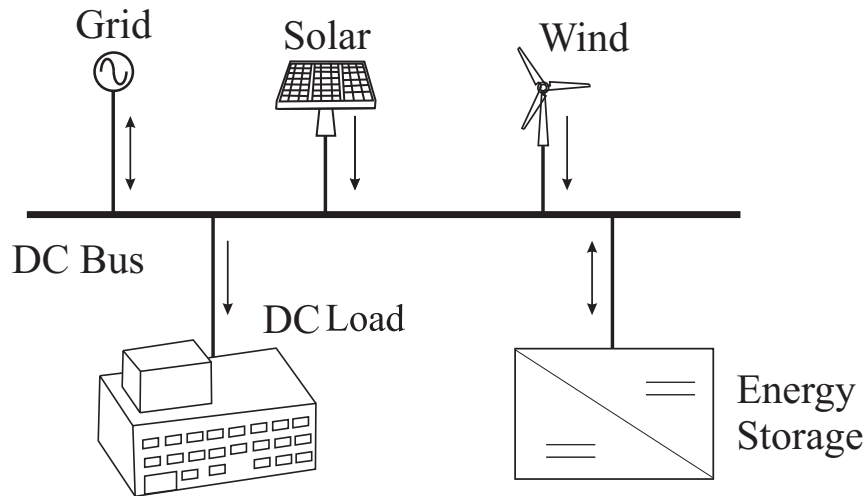
Fig. 1.2. DC microgrid configuration
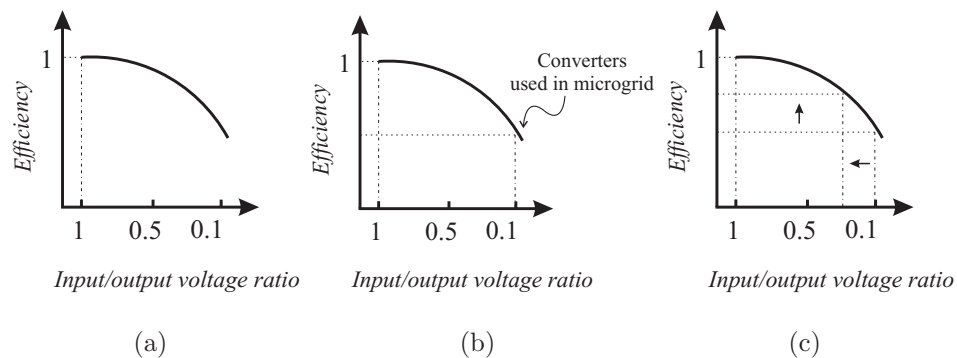
Fig. 1.3. Efficiency of power converters employed in microgrids.

Some works on the technical literature indicate that 380Vdc can be employed for a common bus collecting and distributing DC power in a microgrid scenario. In this case, power converters should be employed to reduce the level of voltage allowing a large variety of loads to be connected to the power line. However, it is worth

mentioning that the efficiency of a power converter is directly affected by both increase and reduction of input-output voltage ratio, as presented generically in Fig. 1.3(a). Notice that, although eliminating AC-DC conversion stages between the power line and load, a DC microgrid experiences the use of a low-efficient power converter. For the sake of illustration lets assume that the DC voltage available at the power line must be reduced by a ratio of 10 to 1. Fig. 1.3(b) highlights the efficiency of the converters employed on this microgrid under the conditions mentioned earlier. Notice that if more than one voltage is available at the power line, it will lead to converters with higher efficiency since a better input/output ratio can be selected, as in Fig. 1.3(c). This is magnified when the number of converters connected to the power line increases. As will be presented in the sequence of this paper, a couple of options of power systems offer the opportunity of using two voltage levels to increase the efficiency of the microgrid system.

Control Methods used for DC Microgrid Link

Diferent control methods have been studied and proposed for the DC microgrid link such as droop control method, control system for data centers, voltage control system for DC link, and etc.

The droop control method is one of the basic methods for controlling the dc microgrid system. In this method the voltage reference will be reduced linearly as the output current increased [29–32]. In [33] it has been proposed a control system for a DC microgrid for data centers. Since the data centers ask for high reliability and reducing the losses and costs, the use of DC microgrid can meet their expectations. This control method will coordinate the control of the two converters in the DC microgrid. In [34] a control method for DC microgrid has been proposed in which the circulating current will be abolished using only the DC voltage. In this method, each unit can be controlled autonomously without contacting each other which will result in higher reliability.

1.1.2   Single-phase Link

Standard 60 Hz Link

The main advantage of designing an electrical power line with a single-phase 60Hz voltage is the physical structure already established in the current power system. Furthermore, the benefits of connecting the microgrid directly to the macrogrid as well as connecting directly a low-power single-phase motor to the line, favors this electrical link. However, many other disadvantages could limit its application as represented in Fig. 1.1. They are: 1) pulsating power flowing on the power line, 2) high dc-link capacitor ripple in a rectifier circuit, and 3) just one voltage level available on the power line.

High-frequency and single split-phase links

An appropriate way to link the renewable energy sources to the loads and grids is to use the single phase high frequency ac-microgrid [35]. Using the high frequency may have some disadvantages such as higher power losses. In [21] it has been shown that the frequency from 400 Hz to 1kHz is suitable for residential applications. As presented in Distributed Intelligent Energy Management System for a Single-Phase High-Frequency AC Microgrid [21], the use of a high-frequency power line with a fundamental frequency of 400Hz is comprehensively used in military and aircraft applications. The requirements on those industries are to reduce size and weight of the components. The use of the high-frequency voltage on the electrical link of the system in Fig. 1 presents some positive and negative aspects. The benefits are: 1) the harmonic components are higher orders than that ones obtained in a 60Hz system, 2) higher luminous efficiency in fluorescent lighting, 3) less dc-link capacitor ripple in diode rectifier circuits, 4) reduced filter sizes, 5) benefits both high-speed motor drives (e.g., 5000 rpm) employed in turbine compressors and blowers as well as melting iron and steel in induction furnace. The disadvantages of the high-frequency

link are: 1) higher power losses and drop voltage on the link, 2) guaranteeing the same flux operation with V/Hz, a motor connected directly to the link will require higher voltage than the ones supplied by a 60Hz link, 3) pulsating power flowing on the power line, 4) just one voltage level available on the power line, and 5) the need of power converters for interfacing the grid. Although the single split-phase has the advantage of furnishing two voltage levels at the power line, allowing higher efficient converters as in Fig. 1.3(c), some challenges remain to make this power system attractive for an application as depicted in Fig. 1.1. These challenges include pulsating power throughout the line and high ripple in a diode rectifier.

1.1.3   Hybrid Microgrid

Recently a hybrid ac/dc microgrid has been studied by [25], which presents the main advantage of furnishing both dc and ac voltages throughout the lines, avoiding either dc-to-ac or ac-to-dc conversions, and improving the efficiency of the whole system. Although the hybrid ac/dc microgrid furnishes two links with different levels of voltage available, it needs four wires to distribute the electrical energy among sources and loads connected to the power line. The hybrid ac/dc microgrid consists of both ac and dc links. That is, when this microgrid is connected to a power converter, both ac and dc links are available at the output [36,37]. Since the deployment of DG systems has been increased, the management of DG systems and the power grid has become a major concern [38,39]. For improving the interconnection of different DG systems and the power grid, the hybrid ac/dc microgrid has been used. In [7] the hybrid microgrid consists of various renewable energy sources has been considered. The hybrid ac/dc microgrid has been proposed in [40] to reduce the number of conversions in ac or dc microgrid. Fig. 1.4 shows the ac and DC links available at the power converters output which is connecting the DG system to the hybrid microgrid.
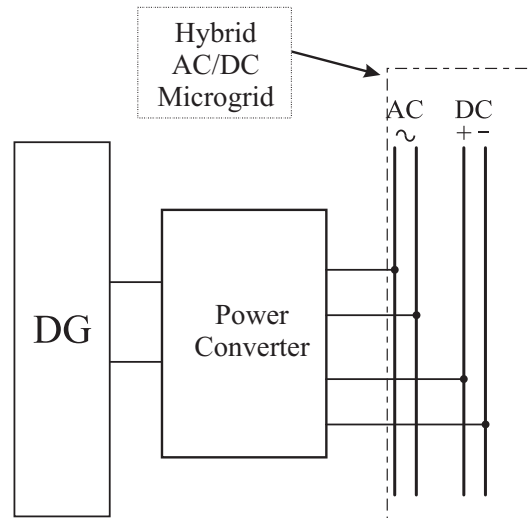
Fig. 1.4. Hybrid Microgrid

Several control strategies have been proposed for using in hybrid Microgrid links, such as : Control of interlinking converter [41, 42], power control and management [43, 44], and etc.

1.1.4 Three-Phase Microgrid

Three-phase microgrid systems can be grouped into two different categories: 1) Three-phase three wire microgrid, and 2) Three-phase four wire microgrid [23, 45]. The three-phase three wire microgrid consists of three lines (phases) and the only voltage available at this kind of microgrid is the line-line voltage. On the other hand, in the three-phase four wire microgrid, 2 voltages are available: the line-line voltage and the phase voltage. As the example of the single-phase 60Hz power system, the three-phase one has the advantage of presenting a physical structure already established in the current power system along with the direct connection to the macrogrid and constant power throughout the line. The ability to supply three-phase motors without power converters can also be cited as one advantage. However, as mentioned earlier, in the idealized microgrid scenario it is expected that the majority of the

motors will be supplied by drive systems, which means power converters interfacing power line and motors. The disadvantages are associated to just one voltage level available while using three wires and the need of ac-dc-ac converters. A three-phase four-wire power link allows the utilization of two voltages levels with a difference of 3 on the amplitude of these voltages. However, it needs four wires. Fig.1.5 shows the three-phase power converter proposed by [46, 47] which uses two conversion stages in order to boost DC voltage and then convert it to a three phase AC voltage. This is power is the conventional bidirectional power converter with eight switches.
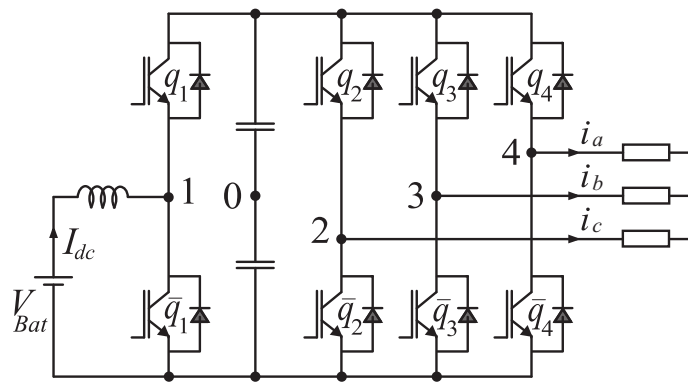
Fig. 1.5. Bidirectional three-phase system

1.1.5 Poly-phase(four-, five-, and six-phase) Link

Although the amount of conductor used in cross-sectional area of each wire reduces by increasing the number phases, as presented in Fig. 3(b), the number of wires is defined by the numbers of phases, which increases complexity and cost to distribute the energy in the microgrid of Fig. 1. Furthermore, the relationship between the number of voltage levels per number of wires is a disadvantage of a poly-phase microgrid system. More details about these systems will be provided in the final version of the paper.

1.1.6 Two-Phase Microgrid

Two-phase microgrid system consists of two voltages (v_α and v_β) in quadrature. Fig. 1.6 shows the two-phase microgrid link. The two-phase microgrid system described in this thesis has the following advantages: 1) constant power at balanced conditions; 2) two voltages available by using a three-wire system, i.e., line-line (V_{ll}) and phase (V_{ph}) voltages with $V_{ll} = \sqrt{2}V_{ph}$; 3) optimized voltage utilization compared to a three-phase system; and 5) direct connection of both symmetrical two-phase and single-phase machines. The main disadvantages of the proposed two-phase microgrid are the need of an interfacing converter to connect the microgrid with the conventional utility grid and the unequal rated currents throughout the wires. The neutral wire dealing with the neutral current must be designed to avoid overheating conditions since it carries 1.414 times the current in the other two phase wires. Two-phase microgrid system has been studied and proposed recently by [48].
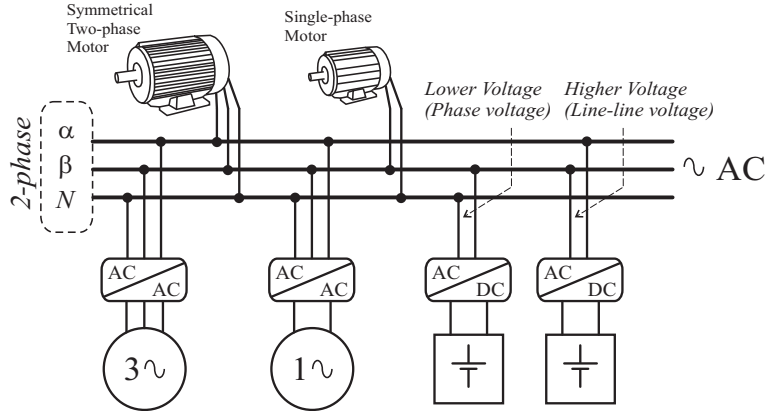
Fig. 1.6. Two-phase microgrid system.

1.1.7 Comparison Among the Previous Electrical Link Architectures

Table 1.1 summarizes the comparison presented in this paper. Notice that, the higher relationship between the number of voltages available per number of wires is

Table 1.1.

Comparison among the power line candidates for the microgrid in 1.1.

Types of MG	Type of power	# of voltages available	# of voltages available/wire	Direct connection to microgrid	DC link capacitor ripple
DC	Constant	1	$\frac{1}{2}$	No	0
Single-phase 60Hz	Pulsating	1	$\frac{1}{2}$	Yes	2.016
Single-phase HF	Pulsating	1	$\frac{1}{2}$	No	0.38
Single Split-phase	Pulsating	2	$\frac{2}{3}$	Yes	4.038
Hybrid	Both	2	$\frac{1}{2}$	No	0
Two-phase	Constant	2	$\frac{2}{3}$	No	2.85
Three-phase 3-wire	Constant	1	$\frac{1}{3}$	Yes	1
Three-phase 4-wire	Constant	2	$\frac{1}{2}$	Yes	1
Poly-phase (4-phase)	Constant	2	$\frac{1}{2}$	No	1.884

for both two-phase and single split-phase. However, the ripple on a diode rectifier as well as the type of power on the line discourages the use of the single split-phase.

1.2 Interconnection of Renewable Energy Sources to the Utility Grid

Now a days central power stations mostly has been replaced by the use of distributed energy resources [49]. Renewable energy sources such as photovoltaic, and wind must be connected to the grid using the power electronics interface such as controlled power electronics converters [50], [51]. These power electronics interfaces are as shown in Fig. 1.7.
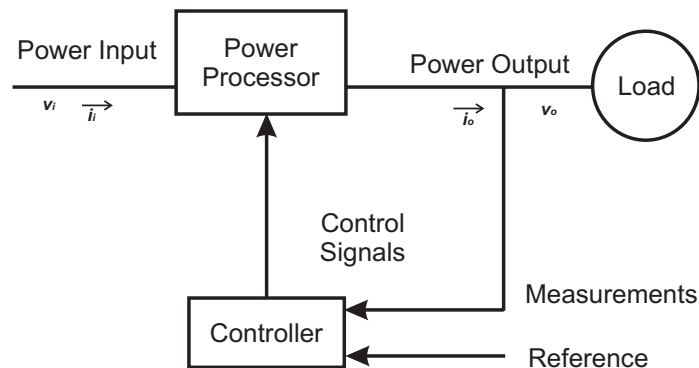
Fig. 1.7. Power Electronic System [50]

1.3   Power Converters

The power processor block shown in Fig. 1.7 consists of different conversion stages which can be referred as a power converter [50]. Power converters consists of energy storage elements such as capacitors, and inductors as well as semiconductor devices such as IGBT switch. In the conversion stage these switches are controlled by the signal electronics [50], [52].

Fig. 1.8 shows an example of a power converter (conversion stage) consists of six semiconductor switches (IGBT), and a capacitor. These power converters may be categorized into broad categories as shown below: [50].

- DC-DC

- DC-AC

- AC-DC

- AC-AC

Some power converters depending on the situation in which they are used can have more than one conversion stage such as:

- DC-DC-AC

- AC-DC-AC

A brief explanation of the DC-DC converter can be found below:

DC-DC power converter can deal with unregulated DC voltage and convert it to a controlled DC voltage. One of the main applications in which the DC-DC converters are used is in DC motor drive applications and renewable energy systems. Based on the desired amplitude for the output DC voltage, these converters can be categorized into either Step-down converter (Buck) [53–55] or Step-up converter (Boost) [56, 57]. In the buck converter the amplitude of the output voltage is less than the input DC voltage and in the boost converter the output is bigger than the input dc voltage [50, 58, 59]. Fig. 1.9 shows the Switch mode DC-DC conversion.
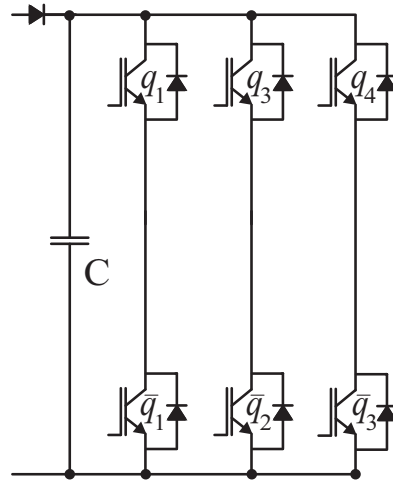
Fig. 1.8. Power Converter [50]
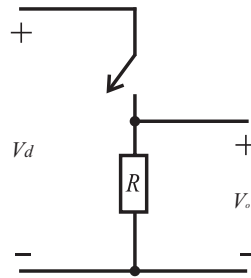
Fig. 1.9. Switch-mode dc-dc Converter [50]

1.4 Power Systems

Since the fossil fuels are running low, the current power systems are coming to an end. For this reason there should be another solution for generating stable power. Sources such as wind, sun, and water are unstable and changeable so it would be hard to get stable power using these sources. Microgrid is a solution for this problem which has advantages such as being automatic, stable, and balanced [60], [61].

2. MICROGRID SYSTEM WITH VOLTAGES IN QUADRATURE

2.1 Introduction

A new concept of microgrid is studied in this chapter, which is based on the two-phase power systems with two voltages in quadrature. The two-phase microgrid system described in this chapter has the following advantages: 1) constant power at balanced condition; 2) two voltages available by using a three-wire system, i.e., line-line (V_{ll}) and phase (V_{ph}) voltages with $V_{ll} = \sqrt{2}V_{ph}$; 3) optimized voltage utilization compared to a three-phase system; and 4) a direct connection of both symmetrical two-phase and single-phase machines. It is worth mentioning that the proposed two-phase microgrid system presents unique advantages that cannot be addressed by either single-phase or three-phase microgrids.

The current research dealing with microgrids has been developed considering the electric power systems available today, such as dc, ac single-phase and mainly ac three-phase systems. However, the first poly-phase electric power system used two phases
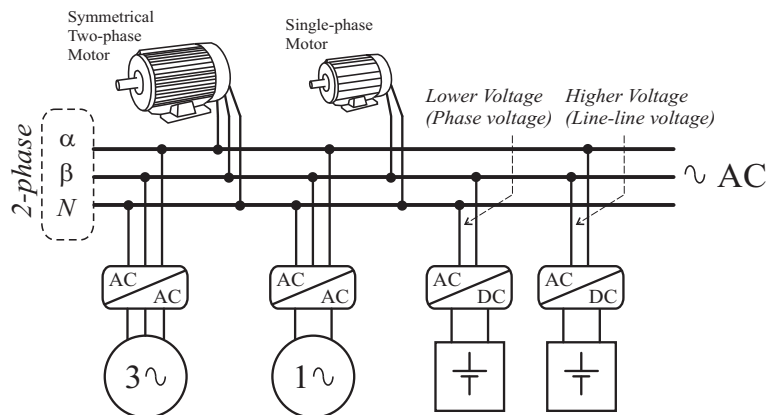
Fig. 2.1. Two-phase microgrid system.

with a 90 degree phase difference, and it was employed during the early 1890s [62]. Westinghouse Electric Corporation employed a two-phase generator for the first ac powerhouse with 25Hz at Niagara Falls when operations started in 1895 [63]. At that time, the use of a two-phase system was motivated by the conviction that it would provide satisfactory voltage regulation [3]. In 1898, the Pacific Light and Power Company installed two-phase generators near Los Angeles, CA [62]. Since the development of the three-phase induction motor has its inherent advantages over the other types of machines, the three-phase system has become the standard commercial type of service provided by electric companies.

However, the recent challenges faced by the power system (e.g., ever-increasing distributed generation and bidirectional power flow) have created an environment in which the old concepts like two-phase systems could be renewed by taking advantage of their features. The characteristics of the two-phase power system are presented in this chapter considering the microgrid point of view. As discussed throughout this chapter, the two-phase microgrid system presents specific advantages when compared to a three-phase system, which has been explored for this application.

2.2   Advantages of the Proposed Microgrid

2.2.1   Constant Power

Among the ac microgrid types available in the technical literature, the single-phase microgrid has an inherent pulsating power, which can restrict the design of this microgrid in terms of the amount of power allowed. On the other hand, dc and three-phase (under balanced conditions) microgrids are characterized by constant power throughout the line. For the two-phase microgrid system, as it is observed in the three-phase system, the instantaneous real power contains only the average power when the voltages and currents comprise only their fundamental positive-sequence

components. In this case, $v_\alpha = V\cos(\omega t)$, $v_\beta = V\sin(\omega t)$, $i_\alpha = I\cos(\omega t + \phi)$, $i_\beta = I\sin(\omega t + \phi)$ and since $P = VI \Rightarrow$

$$p = VI\cos(\phi) \tag{2.1}$$

$$q = VI\sin(\phi) \tag{2.2}$$

2.2.2 Two Voltages Available

In a three-phase system the difference between two phase voltages defines a line-line voltage (with $V_{ll} = \sqrt{3}V_{ph}$), but in a conventional three-phase system both phase and line-line voltages are available only in a three-phase four-wire system (three wires plus neutral wire).

In the case of a three-phase three-wire system, just the line-line voltages are available. The availability of voltages with different amplitudes throughout the line has considerable importance in a microgrid environment. Many of the sources/loads connected to a microgrid have different voltage requirements, which means that the converter's design could be optimized if different voltages were available. The proposed two-phase microgrid presents two voltages available by using only three wires. For this system, the relationship between phase and line-line voltages is given by $V_{ll} = \sqrt{2}V_{ph}$. It is worth mentioning that high-voltage-ratio converters normally have lower efficiency than those with smaller voltage-ratio conversion, which means that either V_{ph} or V_{ll} could be used to avoid high-voltage-ratio converters and increase efficiency of the converters as a whole.

2.2.3 Direct Connection of Two-phase and Single-phase Motors

There are a notable number of low-power applications that employ single-phase machines such as pumps, tools, compressors, fans, and household appliances. The most common form of a typical two-phase machine is the permanent split-capacitor motor, usually recognized as the single-phase induction machine. However, the sym-

metrical two-phase motors represent an interesting solution for low-power applications due to constant power/torque, instead of a pulsating power observed in the single-phase motors [64]. Furthermore, a single-phase motor can still be connected directly to a microgrid line, as observed in Fig. 2.1.

2.3 Interfacing Converter

Fig. 2.2 shows four bi-directional power converters employed to interface single-phase and three-phase utility grids to a two-phase microgrid system. Fig. 2.2(a) shows the conventional solution using five legs, while Fig. 2.2(b) shows the converter with four legs [65], which presents a leg shared (q_3) between the single-phase utility grid and the two-phase microgrid. A direct comparison between the conventional solution and the configurations with a minimized number of components shows a reduction of two power switches. Furthermore, due to the synchronization technique presented in this chapter no voltage restriction is observed for the converters in Fig. 2.2(b) when compared to the one in Fig. 2.2(a).

2.3.1 PWM Control for the Four-leg Converter

The single-phase to two-phase bi-directional converter is made up of four legs. The voltages at the grid side (v_g) and at the two-phase microgrid side (v_α, v_β) are given by:

$$v_g = v_{g0} - v_{30} = (q_g - q_3)E \tag{2.3}$$

$$v_\alpha = v_{10} - v_{30} = (q_1 - q_3)E \tag{2.4}$$

$$v_\beta = v_{20} - v_{30} = (q_2 - q_3)E \tag{2.5}$$

where v_{g0}, v_{10}, v_{20} and v_{30} are the grid and the microgrid terminal voltages and refer to the same dc-bus mid-point.

If the desired phase voltages are given by v_g^*, v_α^*, and v_β^*, then the reference mid-point voltages may be expressed as:

$$v_{g0}^* = v_g^* + v_\mu^* \tag{2.6}$$

$$v_{10}^* = v_\alpha^* + v_\mu^* \tag{2.7}$$

$$v_{20}^* = v_\beta^* + v_\mu^* \tag{2.8}$$

$$v_{30}^* = v_\mu^*. \tag{2.9}$$

The reference voltage set is composed of v_g^*, v_α^*, v_β^* and 0. The voltage v_μ^* was introduced to minimize the voltage distortion.
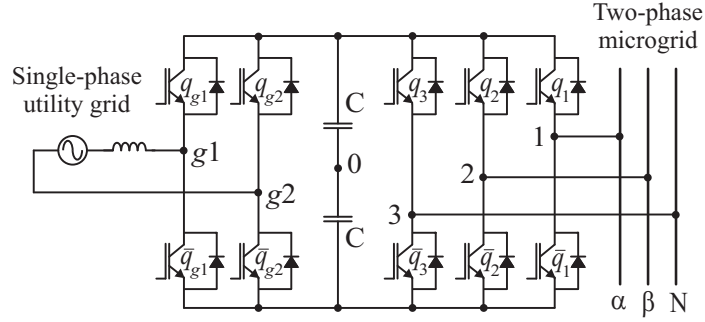
(a)
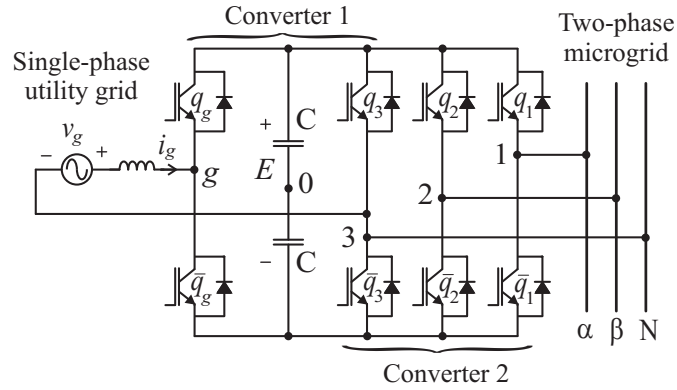
(b)

Fig. 2.2. Bi-directional power converter employed to interface utility grid and a two-phase microgrid system: (a) Conventional solution using five legs for single-phase grid and (b) solution by using four legs for single-phase grid.

The voltage v_μ^* can be calculated taking into account the general apportioning factor μ for both converters 1 and 2 together (converter 1 is composed of switches q_g and q_3 and their complementary switches, while converter 2 is composed of switches q_1, q_2 and q_3 and their complementary switches). In this sense v_μ^* can be given as:

$$v_\mu^* = E(\mu - \frac{1}{2}) - \mu v_{\text{max}}^* + (\mu - 1)v_{\text{min}}^*. \tag{2.10}$$

where $v_{\text{max}}^* = \max V$ and $v_{\text{min}}^* = \min V$ where $V = \{v_g^*, v_\alpha^*, v_\beta^*, 0\}$. This expression was derived by using the same approach as used to obtain the equivalent expression for the three-phase PWM modulator [66], [67].

The apportioning factor μ $(0 \leq \mu \leq 1)$ is given by:

$$\mu = t_{oi}/t_o \tag{2.11}$$

and indicates the distribution of the general free-wheeling period t_o (period in which voltages v_{g0}, v_{s10}, v_{s20} and v_{30} are equal) between the beginning $(t_{oi} = \mu t_o)$ and the end $(t_{of} = (1 - \mu)t_o)$ of the switching period [66], [67].

In this case, the proposed algorithm is:

Step 1. Choose the general apportioning factor μ and calculate v_μ^* from (2.10).

Step 2. Determine v_{g0}^*, v_{10}^*, v_{20}^* and v_{30}^* from (2.6)-(5.12).

Step 3. Finally, once the mid-point voltage have been determined, calculate pulse-widths τ_g, τ_1, τ_2, and τ_3 by using:

$$\tau_j = \frac{T}{2} + \frac{T}{E}v_{j0}^* \quad \text{for} \quad j = g, 1, 2 \text{ or } 3. \tag{2.12}$$

These are accomplished via programmable times or by comparing the modulating reference signal v_{g0}^*, v_{10}^*, v_{20}^* and v_{30}^* to a high-frequency triangular carrier signal.

2.3.2 Synchronization and Control System

The improvement of the voltage rating for the configuration with a shared leg can be obtained by guaranteeing that both input and output converter voltages have the same phase angle.

From (2.3)-(2.5) it can be written:

$$|v_g| \leq E \tag{2.13}$$

$$|v_j| \leq E, \quad j = \alpha \text{ and } \beta \tag{2.14}$$

$$|v_k - v_l| \leq E, \quad k, l = \alpha \text{ and } \beta \text{ and } k \neq l \tag{2.15}$$

$$|-v_g + v_j| \leq E, \quad j = \alpha \text{ and } \beta. \tag{2.16}$$

From (2.13)-(2.16) it can be noted that relations (2.15) and (2.16) determine the maximum single-phase grid and two-phase microgrid voltages that can be generated from a given E.

An additional increase of the voltage rating of the four-leg converter can be achieved by using a type of synchronism between the input (single-phase side) and the output (two-phase side) converter voltages.

Since the maximum voltage difference between two pole voltages is E then $V_g \leq E$, $V \leq E/\sqrt{2}$ and considering that $v_g = -V_g \cos(\omega t - 45^o + \varepsilon)$, $v_\alpha = V \cos(\omega t)$, $v_\beta = V \sin(\omega t)$, the following equations can be derived:

$$V_g^2 + V^2 + 2V_g V \cos(135^o - \varepsilon) \leq E^2 \tag{2.17}$$

$$V_g^2 + V^2 + 2V_g V \cos(225^o - \varepsilon) \leq E^2. \tag{2.18}$$

From (2.17) and (2.18) it can be shown that the maximum V_g and V are, respectively, E and $E/\sqrt{2}$; that is, the same voltage rating of the full-bridge five-leg converter, if:

$$-24.29^o \leq \varepsilon \leq 24.29^o. \tag{2.19}$$

2.3.3   Control System

Fig. 2.3 presents the converter control block diagram. The capacitor dc-bus voltage v_c ($v_c = E$) is adjusted to a reference value by using controller R_c. Since the variables at the link capacitor are dc, a conventional PI controller is enough to guarantee null error. This controller will provide the amplitude of the reference

current I_g^*. To obtain the unity power factor, the instantaneous reference current i_g^* must be synchronized with voltage e_g and with the same phase. This is obtained in block SYN. The current controller is implemented by using a controller indicated by the block R_i. Since i_g is a sinusoidal waveform, a standard PI stationary controller does not guarantee zero steady-state error. The utilization of a double sequence synchronous controller [68] is used to overcome such difficulty.
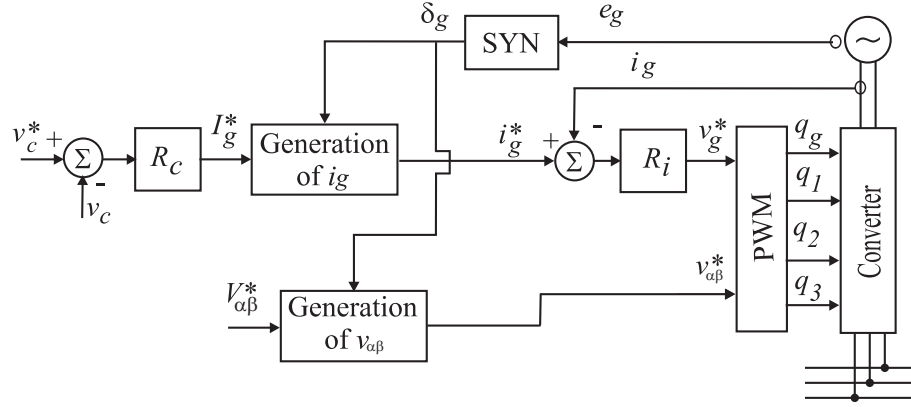
Fig. 2.3. Block diagram of the control scheme.

2.3.4 Shared-leg Current and Power Rating

The average current $\bar{i}_{q3}$ (over the period T) for the switch q_3 can be determined by considering the expression of the pulse-width τ_3 (2.12); then the average current is given by:

$$\bar{i}_{q3} = (\frac{v_{30}^*}{E} + \frac{1}{2})(\bar{i}_g - \bar{i}_\alpha - \bar{i}_\beta)$$

(2.20)

The analysis for switch $\bar{q}_3$ is similar.

When the synchronization is used, the four-leg converter can operate with the same dc-bus voltage of the five-leg converter. The maximum current of the switches q_g, q_1 and q_2 are also the same for the four-leg and five-leg converters. Then the power ratings of switches q_g, q_1 and q_2 are equal in both converters.

The maximum current flowing through q_3 is determined by the sum of the maximum single-phase grid current and two-phase microgrid current.

2.4   Conclusions

A two-phase microgrid system with its power converter interfacing the microgrid itself and the single-phase utility grid has been proposed in this paper. The main advantages of the two-phase microgrid system are: 1) constant power at balanced condition; 2) two voltages available by using a three-wire system, i.e., line-line (V_{ll}) and phase (V_{ph}) voltages with $V_{ll} = \sqrt{2}V_{ph}$; 3) optimized voltage utilization compared to a three-phase system; and 4) direct connection of both symmetrical two-phase and single-phase machines. Besides using a three-wire system, it has been demonstrated that it is possible to use a converter with just four legs to interface the microgrid to the single-phase grid, without reducing voltage capability.

3. SYMMETRICAL COMPONENTS, POWER ANALYSIS, AND HARMONIC ANALYSIS FOR A TWO-PHASE MICROGRID SYSTEM

3.1 Introduction

Fig. 3.1 shows a microgrid being fed by a strong energy source (e.g. wind farm) as well as weak energy sources (e.g., residential PV and smaller wind sources). In
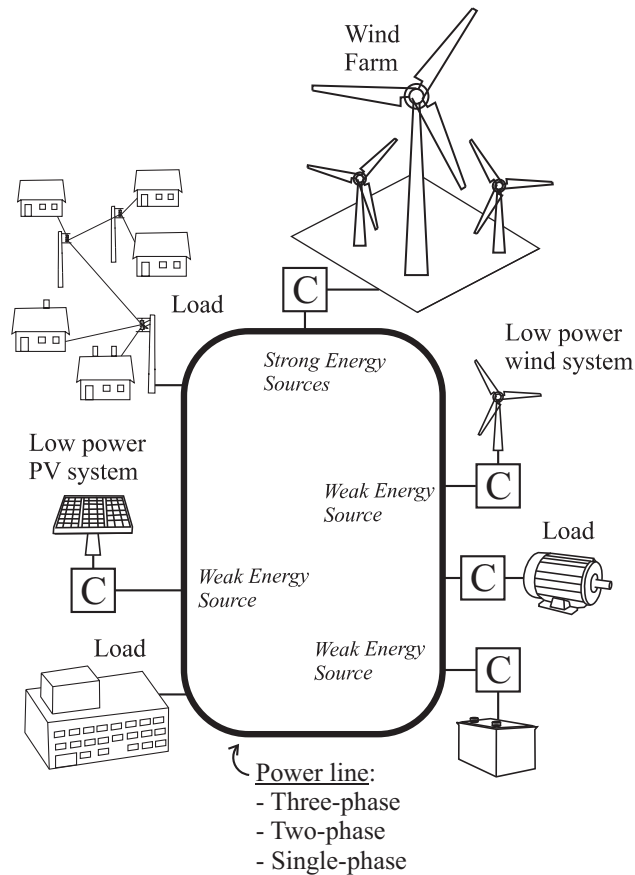
Fig. 3.1. Microgrid environment highlighting the physical electrical link of different sources and loads. C stands for power converter.

Fig. 3.1 the blocks with C mean power converters interfacing the energy sources and the power line. Loads are also spread throughout the line. Research efforts have been developed towards: 1) dc microgrid [19], 2) single-phase 60 Hz ac microgrid [20], 3) single-phase high-frequency ac microgrid [21], 4) three-phase three-wire microgrid [22], 5) three-phase four-wire microgrid [23], and 6) more recently the two-phase microgrid with voltages in quadrature [48]. The physical structure of the power line can also be explored. The two-phase power system presents some advantages as compared to the single-phase and three-phase systems.

This section presents a mathematical model for the symmetrical components and power analysis of the two-phase microgrid system.The method of symmetrical components was first developed for dealing with unbalanced three-phase systems in 1918 by C. L. Fortescue [69].

3.2 Power Analysis

For a two-phase power system, instantaneous voltages v_α and v_β and instantaneous currents i_α and i_β can be expressed as instantaneous space vectors $\overline{v}$ and $\overline{i}$, given respectively by:

$$\overline{v} = \begin{bmatrix} v_\alpha \\ v_\beta \end{bmatrix} \text{ and } \overline{i} = \begin{bmatrix} i_\alpha \\ i_\beta \end{bmatrix} \tag{3.1}$$

The instantaneous active power of a two-phase circuit p can be given by:

$$p = \overline{v} \cdot \overline{i} \tag{3.2}$$

$$p = v_\alpha i_\alpha + v_\beta i_\beta \tag{3.3}$$

where "·" means scalar product of vectors. On the other hand, the vector product of $\overline{v}$ and $\overline{i}$ defines a new instantaneous space vector $\overline{q}$ as follows:

$$\overline{q} \overset{\Delta}{=} \overline{v} \times \overline{i} \tag{3.4}$$

Vector $\overline{q}$ is designated as the instantaneous reactive power vector of the two-phase circuit, or as the nonactive power vector of the two-phase circuit. The magnitude of $|\overline{q}|$ is designated as the instantaneous reactive power, i.e.,

$$q = |\bar{q}| = |\bar{v} \times \bar{i}| \quad \Rightarrow \quad q = v_\alpha i_\beta - v_\beta i_\alpha \tag{3.5}$$

As done for the three-phase power systems and for three-phase microgrids [70], the p and q can be written as:

$$p = \bar{p} + \tilde{p} \tag{3.6}$$

$$q = \bar{q} + \tilde{q} \tag{3.7}$$

where $\bar{p}, \bar{q}$ and $\tilde{p}, \tilde{q}$ represent the average and oscillating components of p and q, respectively. As shown in Fig.3.2, assuming $v_\alpha = V_\alpha \cos(\omega t)$, $v_\beta = V_\beta \sin(\omega t + \varepsilon)$, $i_\alpha = I_\alpha \cos(\omega t + \phi)$, $i_\beta = I_\beta \sin(\omega t + \phi + \varepsilon)$, then the active and reactive powers are given respectively by:
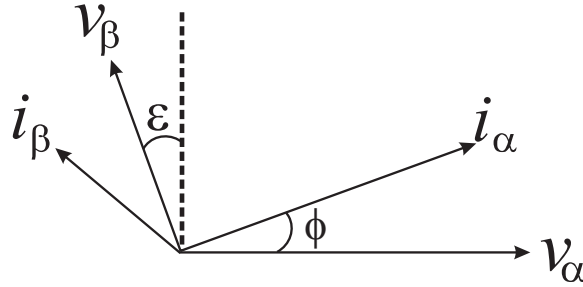
Fig. 3.2. Unbalanced voltages and currents in a two-phase system.

$$p = (\frac{V_\alpha I_\alpha}{2} + \frac{V_\beta I_\beta}{2})cos(\phi)$$
$$+ [\frac{V_\alpha I_\alpha}{2}cos(2\omega t + \phi) - \frac{V_\beta I_\beta}{2}cos(2\omega t + 2\varepsilon + \phi)] \tag{3.8}$$

$$q = \frac{V_\alpha I_\beta}{2}sin(\phi + \varepsilon) - \frac{V_\beta I_\alpha}{2}sin(\varepsilon - \phi)$$
$$+ \frac{V_\alpha I_\beta}{2}sin(2\omega t + \phi + \varepsilon) - \frac{I_\alpha V_\beta}{2}sin(2\omega t + \varepsilon + \phi) \tag{3.9}$$

Considering a balanced case, $V_\alpha = V_\beta = V$, $I_\alpha = I_\beta = I$, and $\varepsilon = 0$ then the instantaneous active and reactive powers are given respectively by:

$$p = VI\cos{(\phi)} \qquad (3.10)$$

$$q = VI\sin{(\phi)} \qquad (3.11)$$

Since the power delivered by the source and the power consumed by the load are constants [Fig. 3.3(a)], there is no low-frequency components on the dc-link capacitors, which benefits its design in terms of the capacitance needed. In the case of a single-phase power line, the pulsating power generated at the source side, as in Fig. 3.3(b), introduces some challenges on the dc-link capacitor design. In this case, the pulsating power coming from the power line goes to the capacitance since the load deals with constant power. A higher capacitance is required as compared to the Fig. 3.3(a).

3.3 Symmetrical Components

The unbalanced phasors of a two-phase system can be resolved into a two balanced system of phasors using their symmetrical sets of components. The symmetrical sets of components in a two-phase system are positive and negative components. The positive sequence of the components consist of two equal phasors in terms of magnitude are in quadrature in terms of angle. These two phasors have the same phase sequence as the original phasors. The negative sequence components also consist of two equal phasors in terms of magnitude and in quadrature in terms of angle. These two phasors have the opposite phase sequence from the original phasors.

If X_α and X_β are two variables (e.g., voltage or current) of the unbalanced two-phase system, then from the above descriptions it can be concluded that:

$$X_\alpha = X_\alpha^{(+)} + X_\alpha^{(-)} \qquad (3.12)$$

$$X_\beta = X_\beta^{(+)} + X_\beta^{(-)} \qquad (3.13)$$
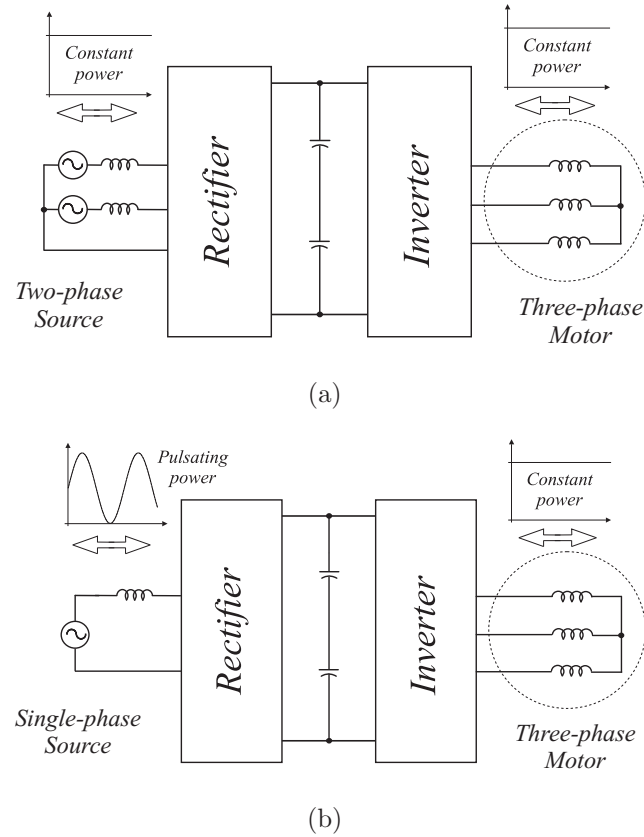
Fig. 3.3. Power processed by a three-phase motor drive system fed by: (a) two-phase and (b) single-phase voltage source.

In (3.12) and (3.13) the superscript (+) refers to the positive component and the superscript (-) refers to the negative component of the phasors.

Fig. 3.4 summarizes the process to obtain the positive and negative components of the two-phase system. In this figure it is obvious that each of the unbalanced vectors is the sum of its symmetrical components as it has been shown in (3.12) and (3.13). For writing the symmetrical components in terms of the unbalanced phasors,

Fig. 3.4. The process of modeling an unbalanced two-phase system using its symmetrical components.

first each component of X_β can be written as the product of a component of X_α and $j = 1\angle 90°$.

$$X_\beta^{(+)} = -jX_\alpha^{(+)} \tag{3.14}$$

$$X_\beta^{(-)} = jX_\alpha^{(-)} \tag{3.15}$$

substituting (3.12) - (3.13) into (3.14) - (3.15) leads to:

$$X_\alpha = X_\alpha^{(+)} + X_\alpha^{(-)} \tag{3.16}$$

$$X_\beta = -jX_\alpha^{(+)} + jX_\alpha^{(-)} \tag{3.17}$$

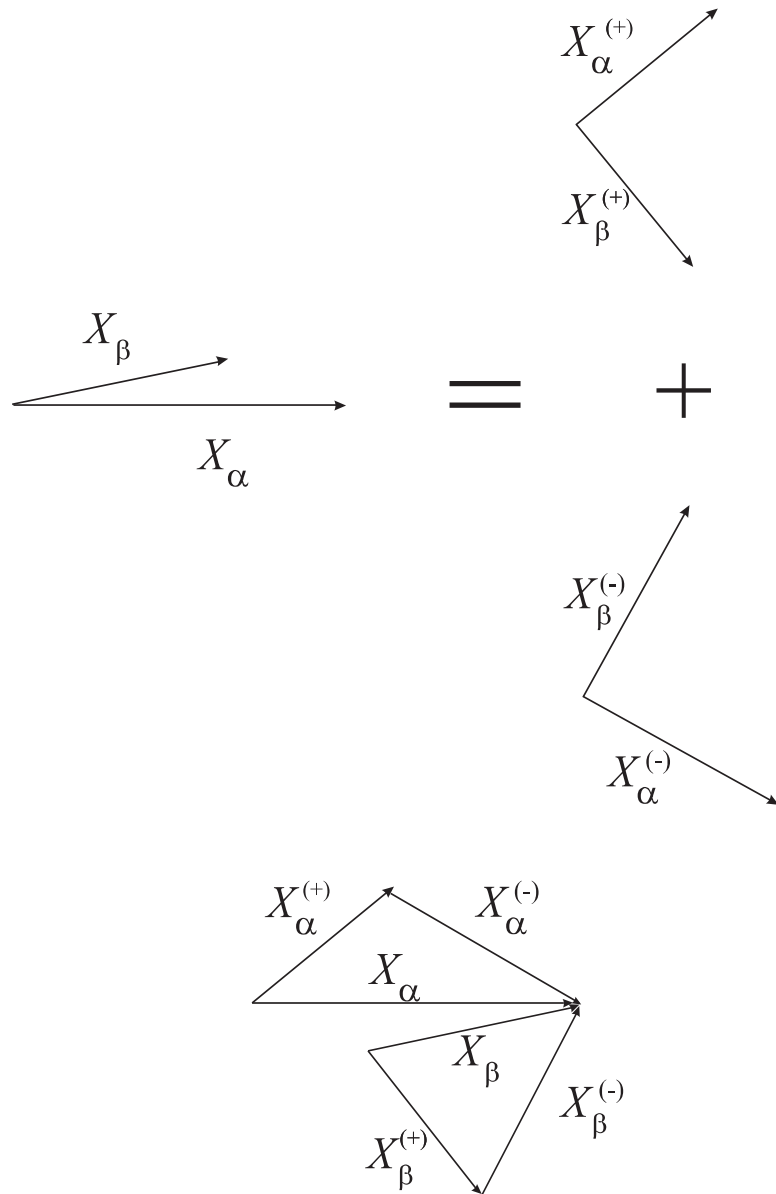It can be concluded from (3.16) and (3.17) that:

$$\begin{bmatrix} X_\alpha \\ X_\beta \end{bmatrix} = A \begin{bmatrix} X_\alpha^{(+)} \\ X_\alpha^{(-)} \end{bmatrix} \tag{3.18}$$

where $A = \begin{bmatrix} 1 & 1 \\ -j & j \end{bmatrix}$

From (3.18) it is obvious that:

$$\begin{bmatrix} X_\alpha^{(+)} \\ X_\alpha^{(-)} \end{bmatrix} = A^{-1} \begin{bmatrix} X_\alpha \\ X_\beta \end{bmatrix} \tag{3.19}$$

where $A^{-1} = \begin{bmatrix} \frac{1}{2} & \frac{1j}{2} \\ \frac{1}{2} & \frac{-1j}{2} \end{bmatrix}$

The process for the symmetrcial component of X_β is similar to the above process with this difference that each component of X_α should be written as a product of a component of X_β with $j = 1\angle90°$.

$$X_\alpha^{(+)} = \frac{1}{2}X_\alpha + \frac{1}{2}jX_\beta \tag{3.20}$$

$$X_\alpha^{(-)} = \frac{1}{2}X_\alpha - \frac{1}{2}jX_\beta \tag{3.21}$$

$$X_\beta^{(+)} = \frac{-1}{2}jX_\alpha + \frac{1}{2}X_\beta \tag{3.22}$$

$$X_\beta^{(-)} = \frac{1}{2}jX_\alpha + \frac{1}{2}X_\beta \tag{3.23}$$

Since the symmetrical components of the α and β are known, the unbalanced two-phase system can be simply represented using (3.12) and (3.13).

3.4   Power Line with Two Voltages Available

In a three-phase system the difference between two phase voltages defines a line-line voltage (with $V_{ll} = \sqrt{3}V_{ph}$), but both phase and line-line voltages are available only in a three-phase four-wire system (three wires plus neutral wire), as observed in Fig. 3.5(a). In the case of a three-phase three-wire system, just the line-line voltages are available, as presented in Fig. 3.5(b).

The availability of voltages with different amplitudes throughout the power line has considerable importance in a microgrid environment. Many of the sources/loads connected to a microgrid have different voltage requirements, which means that the converter's design could be optimized if different voltages were available.

The proposed two-phase microgrid presents two voltages available by using only three wires, as depicted in Fig. 3.5(c). For this system, the relationship between phase and line-line voltages is given by $V_{ll} = \sqrt{2}V_{ph}$. It is worth mentioning that high-voltage-ratio converters normally have lower efficiency than those one with smaller voltage-ratio conversion, which means that either V_{ph} or V_{ll} could be used to avoid low-voltage-ratio converters and increase efficiency of the system as a whole.

A numerical example was considered to demonstrate the importance of having two voltages available in a micro-grid environment. Let's assume the case where a battery (or any other device demanding dc voltage) with a desired dc voltage equal to 310 V (5 kW) must be connected to a three-phase ac link with 220 V RMS (310 V peak), as presented in Fig. 3.6(a). For this particular scenario, the converter loss of the dc-ac conversion stage is equal to 90 W, which includes switching and conduction losses of the power switches [71]. Fig. 3.6(b), on the other hand, shows the case where a 220 V (5 kW) battery must be connected to the same three-phase link. In this case an additional dc-dc power conversion stage must be added to the system to deal with the voltages requirement. As a consequence the power converter loss increases to 145 W.

Table 3.1.
Simulated System for three unbalanced cases in a two-phase microgrid.

Unbalanced Two-phase System	v_α	v_β	$v_\alpha^{(+)}$	$v_\beta^{(+)}$	$v_\alpha^{(-)}$	$v_\beta^{(-)}$
Case 1	$150\angle50°$	$100\angle0°$	$117\angle65.83°$	$117\angle-24.17°$	$48.78\angle8.78°$	$48.78\angle90.878°$
Case 2	$150\angle0°$	$150\angle100°$	$13.073\angle-85°$	$13.073\angle-175°$	$149.429\angle5°$	$149.429\angle95°$
Case 3	$100\angle0°$	$150\angle90°$	$25\angle180°$	$25\angle90°$	$125\angle0°$	$125\angle90°$

The dc-dc converter, and consequently its additional losses, can be eliminated if the proposed two-phase micro-grid system is employed, as observed in Figs. 3.6(c) and 3.6(d). Fig. 3.6(c) shows the case where the higher voltage (310 V) is required for the dc side, which means that the ac side of the converter should be connected to the line-to-line of the ac link. Fig. 3.6(d), in turn, shows the case where the lower voltage (220 V) is required for the dc side, meaning that the ac side of the converter should be connected to the phase voltage of the ac link.

3.5 Simulated Results

Fig. 3.7 shows the simulation results obtained to validate the method proposed for two-phase symmetrical components. Fig. 3.7(a) shows an unbalanced set of voltage in a two-phase system with different amplitudes and an angle displacement of 50 degrees.

Figs. 3.7(b) and 3.7(c) show the symmetrical components obtained in Section III for the voltages in Fig. 3.7(a). For validation purposes, such symmetrical components are added together and the result is shown in Fig. 3.7(d). Notice that Figs. 3.7(a) and 3.7(d) are identical. This case is being shown in Table I as case 1, which indicates the values obtained for symmetrical components of v_α and v_β. In Table I, there are two other unbalanced cases: case 2, both vectors have the same amplitude of 150 V and the angle difference of $\angle100°$, and case 3, is the case in which two vectors are balanced in terms of angle but they have different amplitudes.

Three-phase Four-wire System

Three-phase Three-wire System

(a)

(b)

Two-phase Three-wire System

(c)
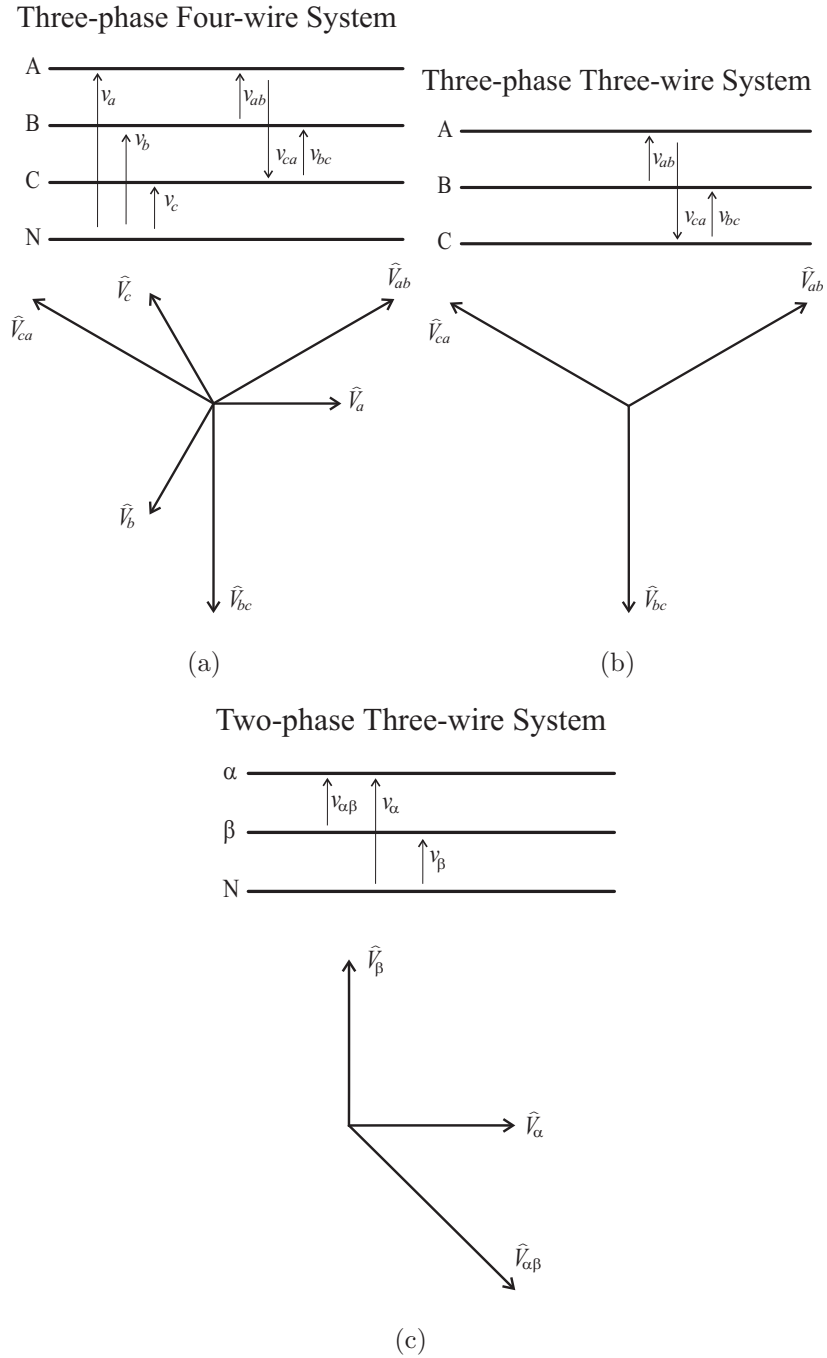
Fig. 3.5. Voltages availability for: (a) three-phase four-wire system, (b) three-phase three-wire system, and (c) two-phase three-wire system.
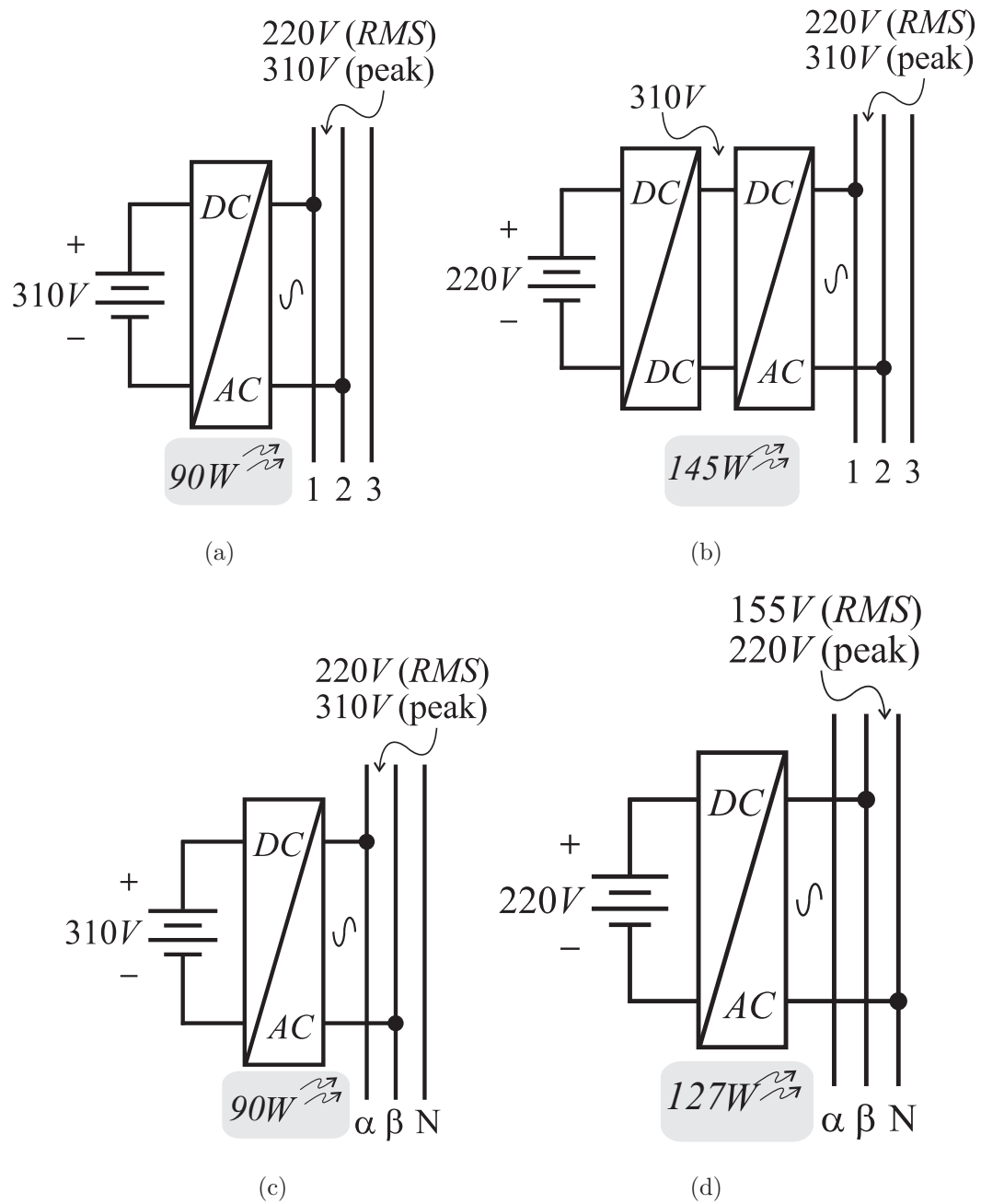
Fig. 3.6. Interconnection between dc and ac variables with three-phase microgrid for: (a) higher and (b) lower voltages; and with two-phase microgrid for: (c) higher and (d) lower voltages.

For the three-phase system, the major cause of voltage unbalance is the uneven distribution of single-phase loads, that can be continuously changing across a three-

phase link [72]. The single-phase loads are equally distributed among the phases to minimize the unbalance caused by this type of load. Sometimes there is no combination among the single loads to avoid a system unbalance.

A simple example has been used in Fig. 3.8 and Fig. 3.9 to illustrate the scenario in which an unbalanced system is inevitable for the three-phase system. But it does not cause unbalance for the two-phase system. Fig. 3.8(a) shows two single-phase loads connected to the three-phase link. Fig. 3.8(b) shows the balanced three-phase voltages among the three-phase link. Fig. 3.8(c) shows the three-phase currents among the three-phase link and as it is shown in this figure, the currents are unbalanced due to the even number of distributed loads. Fig. 3.8(d) shows the pulsating power among the three-phase link. This ends up as an unbalanced system. However, if the two-phase link is employed, it leads to a balanced system, as in Fig. 3.9(a). Fig. 3.9(b) and 3.9(c) show the balanced two-phase voltages and currents. In this case unlike the three-phase link, the currents are also balanced due to the even number of distributed loads. Fig. 3.9(d) shows the power among the two-phase link, and as expected this power is a constant. On the other hand, if an odd number of single-phase loads are considered, the three-phase solutions are likely to present advantages as compared to the two-phase system.

3.6   Harmonic Analysis

This paper presents a time domain method to analyze the harmonics content in a two-phase microgrid system. With this analytical method it is possible to evaluate harmonics and compare the two-phase system with a single-phase and three-phase systems. The proposed two-phase microgrid presents the following advantages: 1) constant power at balanced conditions, instead of a pulsing power in the single-phase microgrid; 2) two voltages available by using a three-wire system, i.e., line-line (V_{ll}) and phase (V_{ph}) voltages with $V_{ll} = \sqrt{2}V_{ph}$; 3) lower voltage fluctuation as compared to the single-phase system at the dc-link voltage of a Voltage Source Inverter (VSI)

fed drive; and 4) a direct connection of both symmetrical two-phase and single-phase machines. A practical implementation of the two-phase system has been performed where different type of loads are connected to the two-phase power line to test the voltage control performance.

Rectifiers mainly inject significant current harmonics to the power network with harmful impacts on the power systems. These harmonics should be predictable to determine how they will interact with other components in the power system. In this section, the single-phase, two-phase, and three-phase rectifiers have been analyzed in terms of harmonics. Figs. 3.10(b), 3.10(c), and 3.10(d) show the single-phase, two-phase, and three-phase rectifier, respectively.

Figs. 3.11(a), 3.11(b), and 3.11(c) show the waveforms of the rectifiers in Fig. 3.10, these waveforms are in pu. Fig. 3.11(a) shows the input voltage v_s, current i_s and the dc-link voltage V_o for the single-phase rectifier. Fig. 3.11(b) shows the line-line voltages $v_{\alpha\beta}$ and $v_{\beta\alpha}$, currents i_α and i_β and the dc-link voltage V_o for the two-phase rectifier. Fig. 3.11(c) shows six line-line voltages, the dc-link voltage V_o for the three phase rectifier and the currents i_a, i_b, and i_c for the three-phase rectifier.

The terms γ and η in Fig. 3.11 show the instant at which the conduction will begin and the conduction interval, respectively. According to [73] and [74] one can analyze the harmonics of single-phase and three-phase rectifier based on the Fast Time Domain Method and the Sampled-Data Model from γ and η. In the two-phase diode rectifier, there is no current going through the neutral line, as explained in Fig. 3.12(a). In notice from Fig. 3.12(a) that the phase voltages are always smaller than the line-line voltages. As a consequence the diodes connecting to the neutral line will never be on and according to this fact the current through the neutral line will be always equal to zero.

Fig. 3.12(b) shows the equivalent circuit of a two-phase rectifier in half of one period. The corresponding differential equations for the conduction and nonconduction interval are given in (3.24).

$$\frac{d}{dt}\begin{bmatrix} i_d \\ v_o \\ v_\alpha \\ v_\beta \end{bmatrix} = A \times \begin{bmatrix} i_d \\ v_o \\ v_\alpha \\ v_\beta \end{bmatrix} \tag{3.24}$$

Where $A = \begin{bmatrix} \frac{-R_d}{L} & \frac{-1}{L} & \frac{1}{L} & \frac{-1}{L} \\ \frac{1}{C} & \frac{-1}{CR} & 0 & 0 \\ 0 & 0 & 0 & -\omega \\ 0 & 0 & \omega & 0 \end{bmatrix}$.

In this case the diode will be modeled as a variable resistor (R_d), so when the diode is on it will be equal to R_{on} and when it is off it will be equal to R_{off}.

Using equation (1), diode constraint equations, and the steady state equations one can determine the intervals γ and η which will be found using the newton-type iterative method. Once the intervals γ and η are found, one can solve for the current and voltage harmonics injected by a two-phase rectifier. More details will be presented in the final version of the paper.

3.7 Conclusion

The symmetrical components and power analysis of a new microgrid system consisting of three wires and two voltages in quadrature are proposed in this paper. The main advantages of the two-phase microgrid system are: 1) constant power at balanced condition; 2) two voltages available by using a three-wire system, i.e., line-line and phase voltages; 3) optimized voltage utilization compared to a three-phase system; and 4) direct connection of both symmetrical two-phase and single-phase machines. Also, it was demonstrated that two voltages available at two-phase microgrid system lead to avoid low-voltage-ratio converters and increase efficiency of the system as a whole.
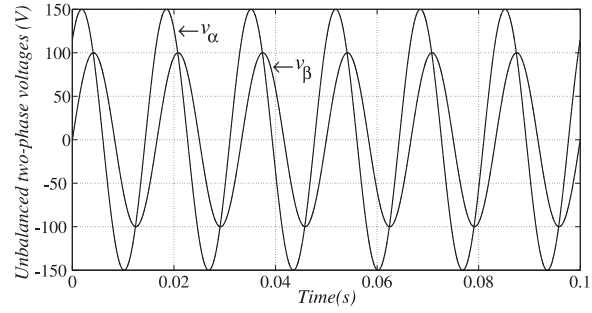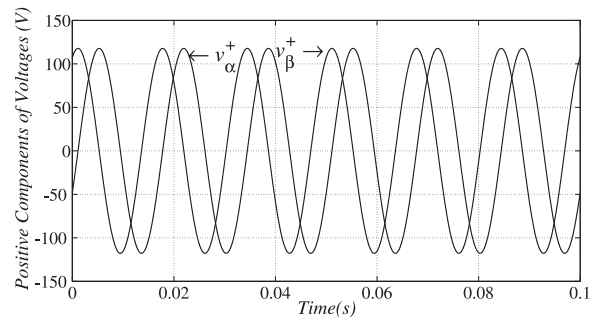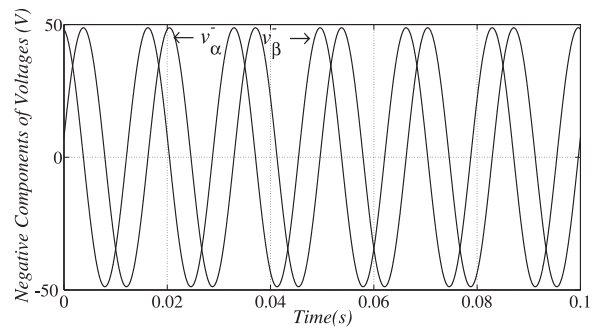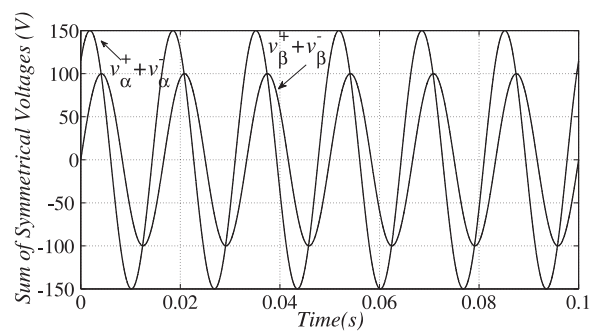
Fig. 3.7. Unbalanced two-phase system: (a) two unbalanced vectors, (b) Symmetrical Positive Components, (c) Symmetrical Negative Components, and (d)two sets of symmetrical components.
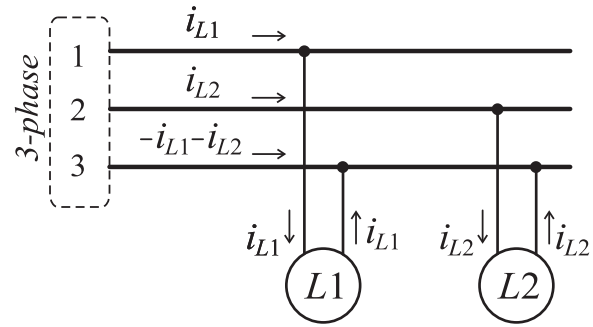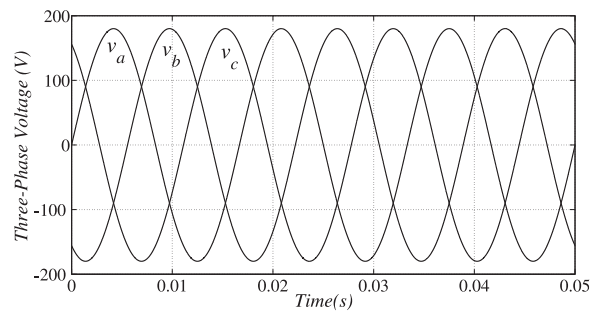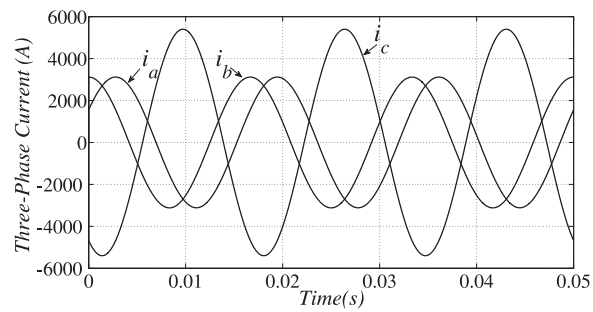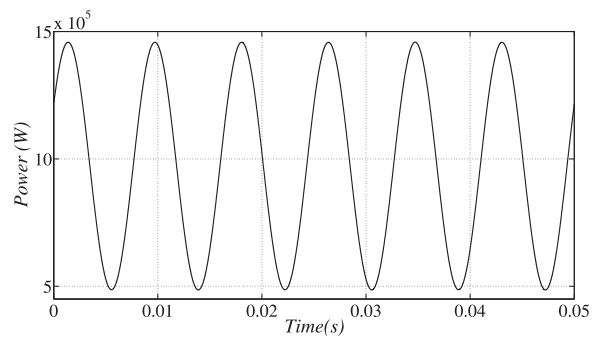
Fig. 3.8. Simulation of Three-phase System, (a) Three-Phase Link, (b) Three-Phase Balanced Voltages, (c) Three-Phase Unbalanced Currents, (d) Power at the Three-Phase Link.
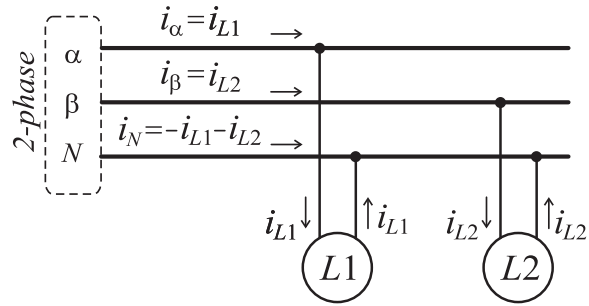
(a)
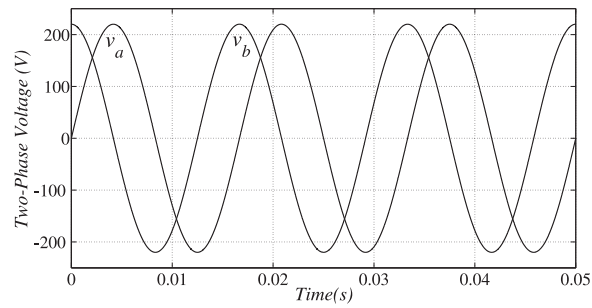
(b)
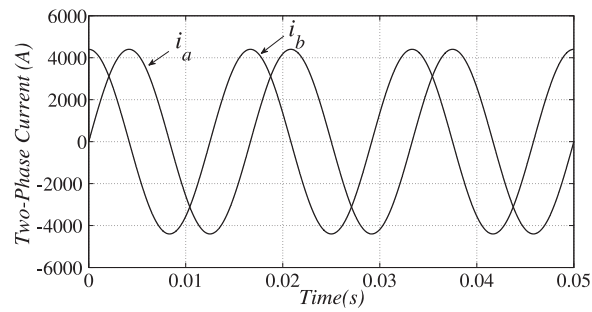
(c)
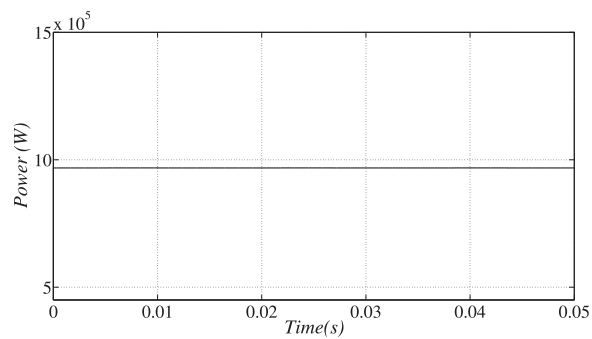
(d)

Fig. 3.9. Simulation of Two-phase System, (a) Two-Phase Link, (b) Two-Phase Balanced Voltages, (c) Two-Phase Balanced Currents, (d) Power at the Two-Phase Link.
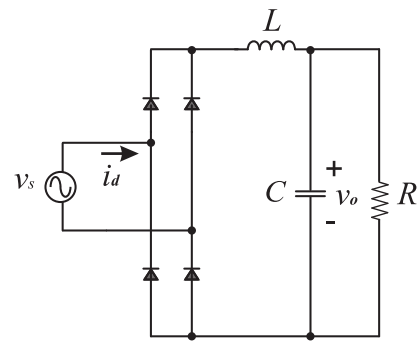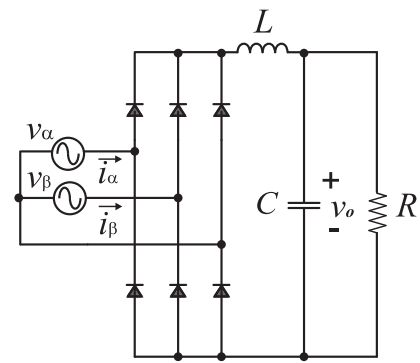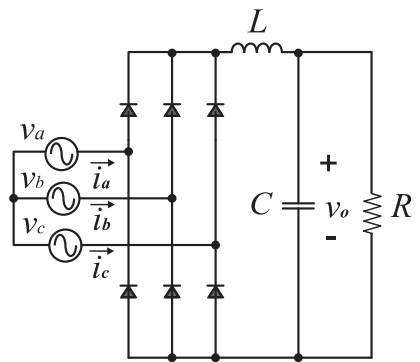
Fig. 3.10. (a) Single-phase rectifier (b) Two-phase rectifier (c) Three-phase rectifier.
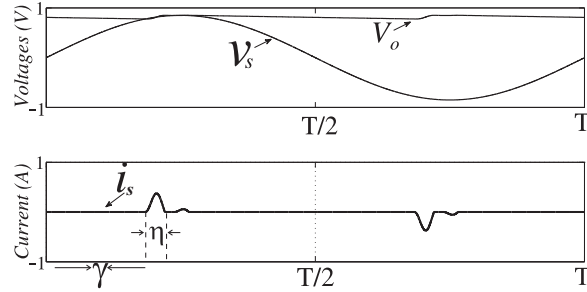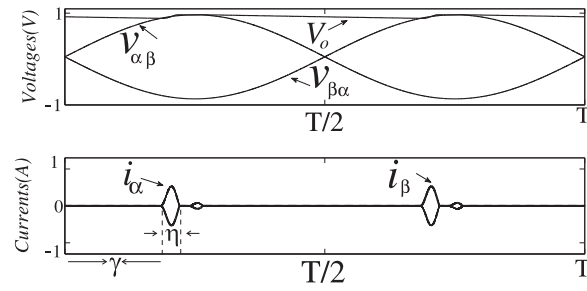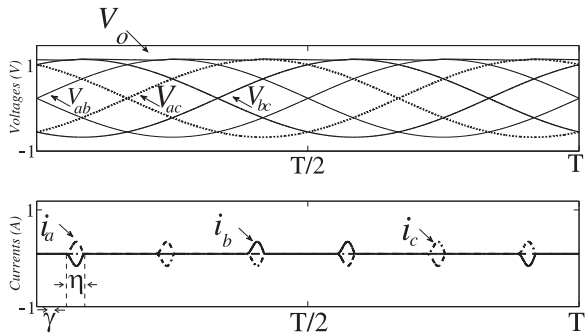
Fig. 3.11. Main normalized waveforms of the: (a) single-phase, (b) two-phase, and (c) three-phase rectifiers.
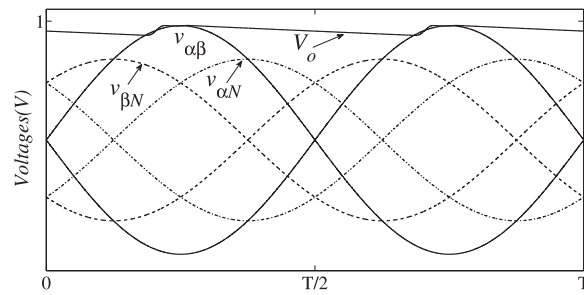
(a)
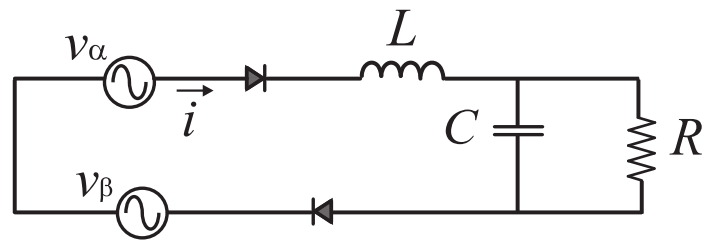
(b)

Fig. 3.12. (a) Line-line, phase, and output voltage for two-phase system. (b) Equivalent circuit for two-phase system in one period.

4. NEW POWER ELECTRONIC CONVERTER INTERFACING A DG SYSTEM WITH HYBRID DC/AC MICROGRID

This chapter mainly discussed a new topology of power electronics converter able to connect a distributed generation (DG) system with a hybrid dc/ac microgrid, as shown in Fig. 4.1(a). Fig. 4.1(b) shows the conventional power electronics converter for the same application. The main advantage of the new converter is high level of integration with reduction of one power switch, while keeping the same features of the conventional solution, such as (i) bidirectional power flow between dc and ac micro-grids, (ii) independent control in both dc and ac parts, and (iii) different operation conditions using a unique power conversion circuit. Despite proposing a new solution, this chapter presents an analysis of the converter in terms of its operation and PWM strategy, as well as the analysis of the power flow among different elements employed in the system.

4.1 Converter Description

The proposed converter is composed of five power switches q_{1a}, q_{2a}, q_{3a}, q_{1b} and q_{2b} arranged in only two legs. The first leg is constituted by three switches q_{1a}, q_{2a} and q_{3a} while the second one is composed of only two switches q_{1b} and q_{2b}.

A binary variable is associated with each switch, (i.e., $q_{xy} = 1$ is used when the switch is closed, and $q_{xy} = 0$ when the power switch is open, with $x = 1, 2, 3$ and $y = a, b$). Notice that, as observed in the conventional converter (with two switches per leg), the switches in the three-switch leg cannot be turned on simultaneously, which will avoid a short-circuit through dc-link capacitor. Eight possible switching states could be obtained for this leg, since there are three switches with two switching
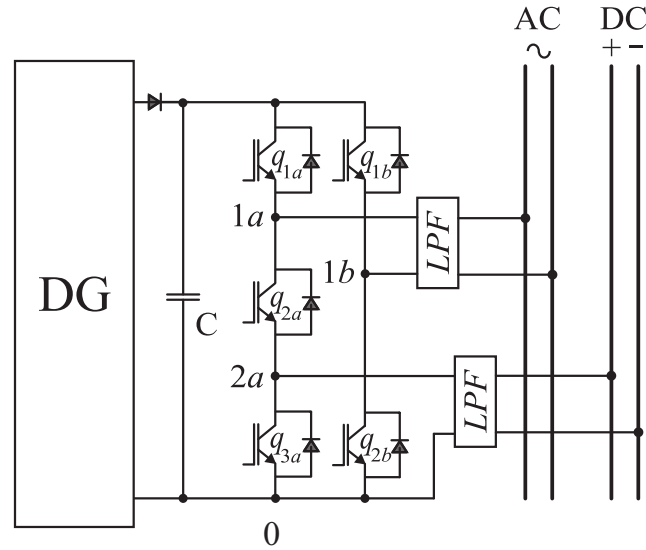
(a)
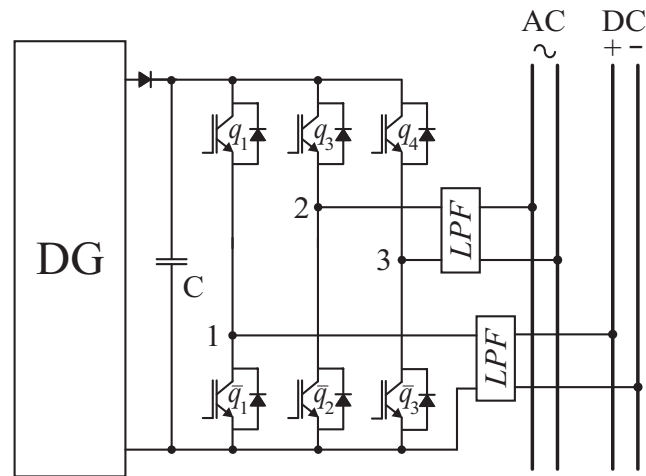
(b)

Fig. 4.1. Bidirectional converter interfacing DG system, hybrid dc and ac micro-grid: (a) proposed solution with five switches and (b) conventional solution with six switches.

states each ($q_{xy} = 1$ and $q_{xy} = 0$). Many of these switching states are prohibited, because of either a short-circuit or one of the unwanted switching states. For instance, when trying to generate lower voltage at point $1a$ [see Fig. 4.1(a)] than that at point $2a$. Table 4.1 shows all possible states with the indication of no-prohibited states.

Table 4.1.

Indication of prohibited switching states of three-switch leg.

States	q_{1a}	q_{1b}	q_{1c}	Prohibited States
1	0	0	0	Yes
2	0	0	1	Yes
3	0	1	0	Yes
4	0	1	1	No
5	1	0	0	Yes
6	1	0	1	No
7	1	1	0	No
8	1	1	1	Yes

From Table 4.1 it is possible to write the equations to model the three-leg switch, as follows:

$$v_{1a0} = [q_{1a}(1 - q_{2a}q_{3a})]V_{Cap} \qquad (4.1)$$

$$v_{2a0} = [q_{1a}q_{2a}(1 - q_{3a})]V_{Cap} \qquad (4.2)$$

where V_{Cap} is the capacitor voltage connected to the DG system.

In order to define the voltages at dc and ac converter sides, it is necessary to write the voltage at the second leg, (i.e., v_{1b0}), which is given by:

$$v_{1b0} = q_{1b}V_{Cap} \qquad (4.3)$$

or

$$v_{1b0} = (1 - q_{2b})V_{Cap} \qquad (4.4)$$

Once the voltages v_{1a0}, v_{2a0} and v_{1b0} are defined, it is possible to write the voltages at dc and ac converter sides, as follows:

$$V_{dc} = v_{2a0} = [q_{1a}q_{2a}(1 - q_{3a})]V_{Cap} \tag{4.5}$$

$$v_{ac} = v_{1a0} - v_{1b0} = [q_{1a}(q_{2a} + q_{3a}) -$$

$$2q_{1a}q_{2a}q_{3a} - q_{1b}]V_{Cap} \tag{4.6}$$

Fig. 4.2 shows the equivalent circuits of the proposed configuration, highlighting how each voltage has been obtained for both converter sides. For the dc side, just two values are possible either $V_{dc} = 0$ [see Figs. 4.2(a)-4.2(d)] or $V_{dc} = V_{cap}$ [see Figs. 4.2(e)-4.2(f)], while for the ac converter side, three values are verified: $v_{ac} = 0$ [see Figs. 4.2(a), 4.2(d) and 4.2(f)], $v_{ac} = V_{cap}$ [see Figs. 4.2(c) and 4.2(e)], or $v_{ac} = -V_{cap}$ [see Fig. 2(b)] which allows this side of the converter to generate ac voltage.

4.2 PWM Strategy

The gating signals of the switches must be obtained to avoid the prohibited states as well as to guarantee independent control at both converter sides. Notice that all gating signals of switches employed in the proposed configuration are obtained directly from the comparison of reference voltages v_{ac}^*, V_{dc}^* (and combination of both) with the triangular waveform, as observed in Fig. 4.3(a).

It is worth mentioning that, for the leg with three switches it is not possible to generate lower voltage at point $1a$ (see Fig. 4.1) than that at point $2a$. In the same way, it is not possible to produce a higher voltage at point $2a$ than that at point $1a$. This can be implemented just by adding an offset value in the reference of the ac voltage, as done in Fig. 4.3(a). The reference waveforms used for PWM generation are presented in Fig. 4.3(b).

If the desired voltages for the dc and ac converter sides are given respectively by V_{dc}^* and $v_{ac}^* = V_{ac}^* \cos(\omega t + \theta)$, where V_{ac}^* is the peak value of the reference voltage, then
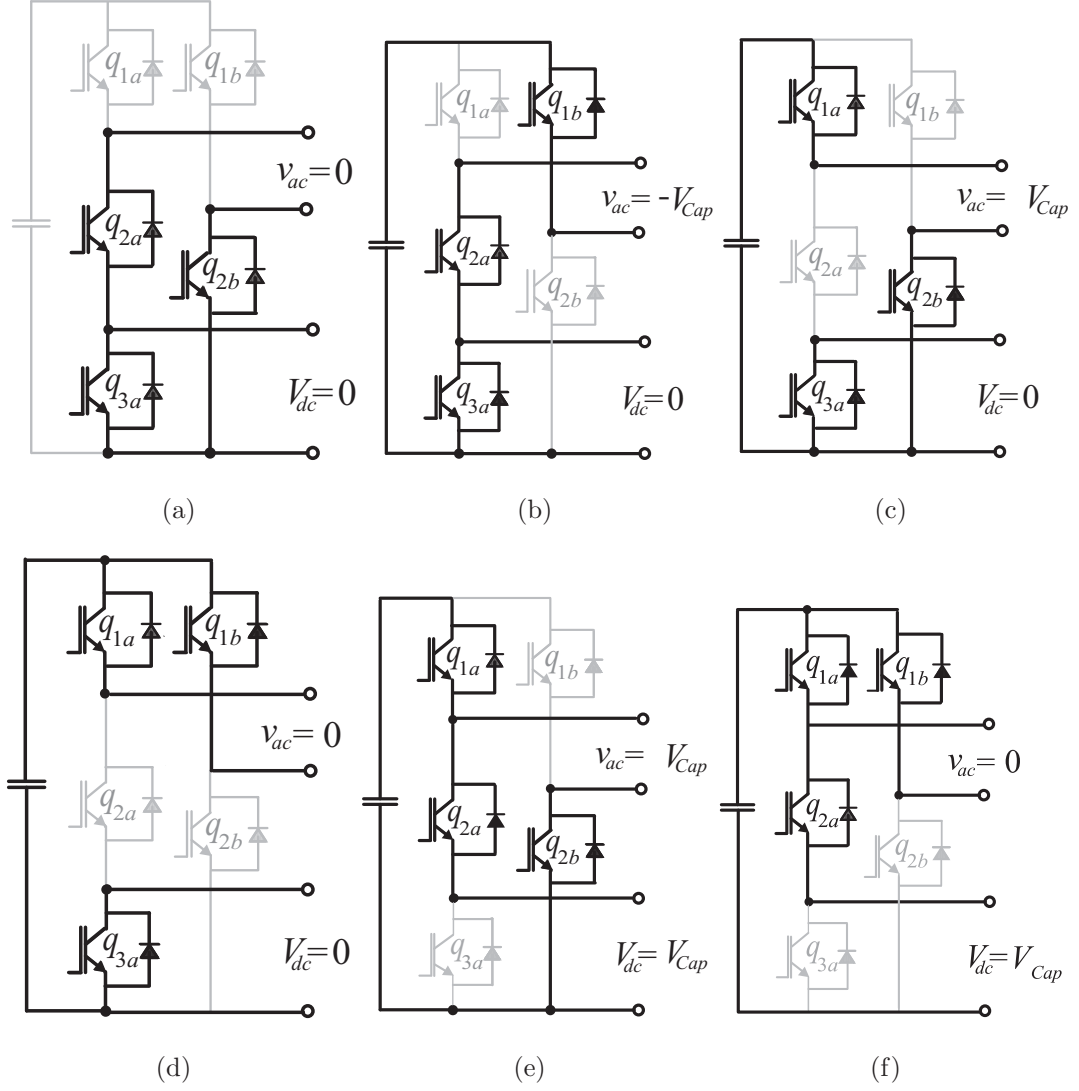
Fig. 4.2. Equivalent circuits of the proposed configuration (The converter with five switches).

the reference voltages from the points $1a$, $2a$ and $1b$ to the point 0 may be expressed as:

$$v_{2a0}^* = V_{dc}^* \tag{4.7}$$

$$v_{1a0}^* = \frac{v_{ac}^*}{2} + V_{offset}^* \tag{4.8}$$

$$v_{1b0}^* = -\frac{v_{ac}^*}{2} + V_{offset}^* \tag{4.9}$$
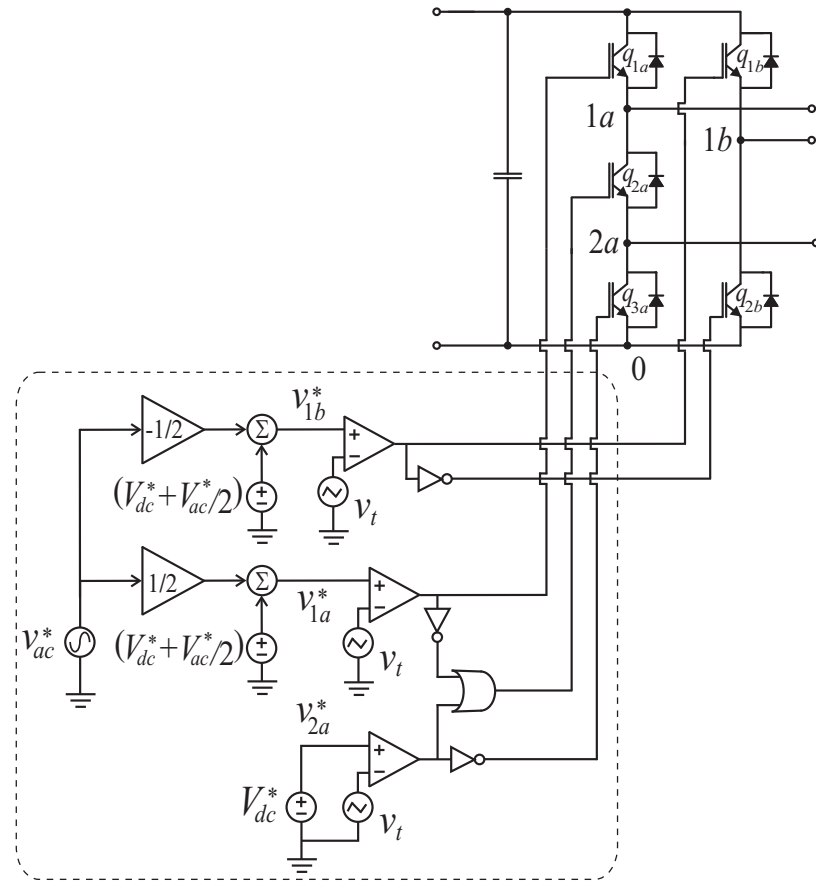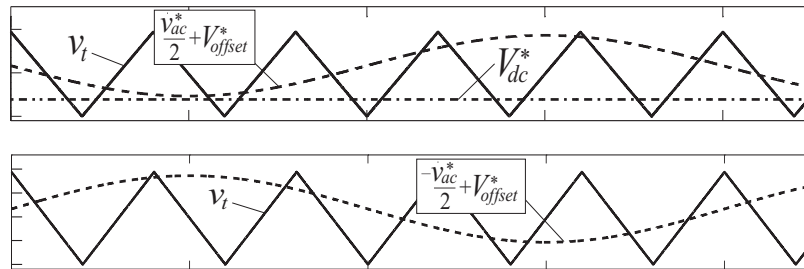
Fig. 4.3. (a) PWM scheme. (b) PWM waveforms for the proposed converter.

where V^*_{offset} is the voltage to avoid the prohibited states, with $V^*_{offset} = V^*_{dc} + V^*_{ac}/2$. The amplitude modulation ratio for the proposed converter can be defined as $m_a = 2V^*_{ac}/(V^*_{Cap} - V^*_{dc})$.

Once the reference voltages have been determined, the pulse-widths and consequently gating signals can be generated with programmable timers for a digital implementation. Alternatively, the gating signals can be generated comparing modulating reference signals v_{2a0}^*, v_{1a0}^* and v_{1b0}^* with a high frequency triangular carrier signal, as observed in Fig. 4.3(a).

4.3   Modes of Operation

Fig. 4.4 shows the sketch maps of the energy flow under different operation modes. This figure highlights the energy flow among the three elements found in the hybrid dc and ac linked micro-grid. In Mode I ac and dc links are demanding energy from the DG, while in Mode II the dc micro-grid is demanding energy while the ac link is not connected anymore. Mode III is the mode in which ac link is demanding energy while the dc link is disconnected. Mode IV and V are two modes in which ac and dc microgrids are generating power to the system respectively. As observed in Fig.4.4 the ac and dc links can either deliver or receive energy or still be out of operation; i.e., no energy is received or delivered. On the other hand, the energy flow in the DG is unidirectional (e.g., photovoltaic panel and wind turbine followed by a diode rectifier), which means that this element cannot receive energy. Both proposed and conventional converters (Fig. 4.1) are able to deal with all operation modes in Fig. 4.4.

4.4   Power Management

As discussed in Section IV, this converter can operate in five different modes. In Fig. 4.4(d) and 4.4(e) the ac and dc grids are generating instead of consuming power, respectively. The power management for these two modes are described below.
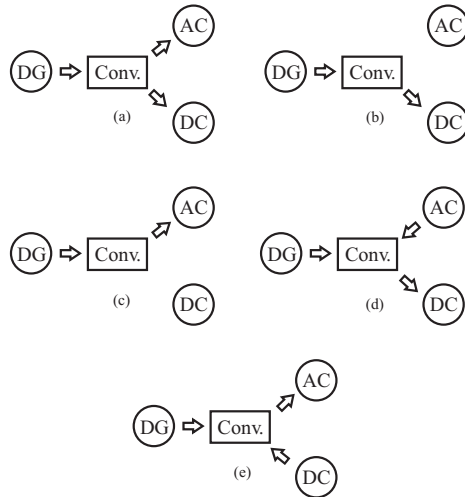
Fig. 4.4. Sketch maps of the energy flow under different operation modes, where DG-Distributed Generation, AC -ac micro-grid, DC - dc micro-grid. (a) Mode I (b) Mode II (c) Mode III (d) Mode IV (e) Mode V.

4.4.1 Mode IV

In Fig. 4.4(d), the ac grid is sending energy to the converter plus dc microgrid. It has been used a phase-angle control to deal with the amount of ac energy either delivered or received by the ac microgrid.

Fig. 4.5(a) shows an equivalent circuit highlighting the ac variables of the system. In this figure $\hat{V}_{ac}$, $\hat{I}_{ac}$ and $\hat{V}_{PCC}$ are the phasors for v_{ac}, i_{ac} and the voltage at the PCC (Point of Common Coupling), respectively. X_{ac} is the equivalent impedance for the LPF.

Fig. 4.5(b) shows the phasor diagram for the variables presented in Fig. 4.5(a). The power between the ac grid and converter can be calculated by using 4.10. Notice that by controlling (θ), it is possible to change the power either received or delivered by the ac microgrid.

$$P = \frac{V_{ac}V_{MG}}{X_{ac}}sin\theta. \tag{4.10}$$
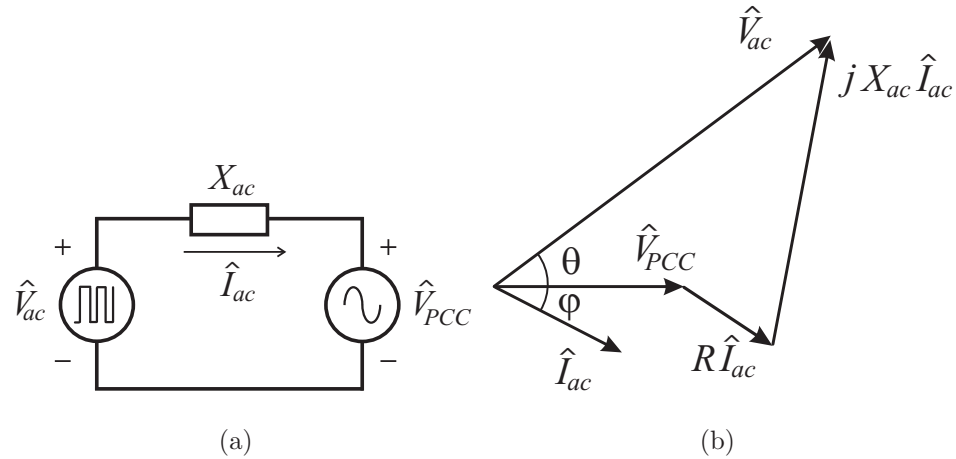
Fig. 4.5. (a) Equivalent circuit for ac variables. (b) Phasor diagram.

4.4.2 Mode V

In Fig. 4.4(e), is shown a mode in which the dc micro-grid is generating instead of consuming power. In this mode there has been used a PI controller in order to control the dc current and consequently the power. Fig. 4.6 shows a closed loop control block diagram. In this figure the dc current is compared with the reference current and applied to a PI controller. The output of the PI controller will be the input voltage of the converter.
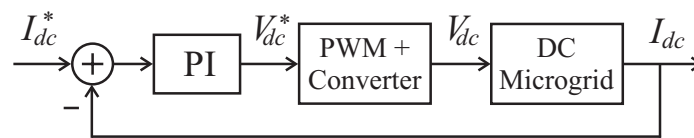
Fig. 4.6. Control block diagram for dc variables.

4.5 Low Pass Filter

By using Kirchhoff's law for the LCL filter as shown in Fig. 4.7, it yields:

$$i_{ac} - i_c - i_g = 0 \tag{4.11}$$

$$v_{ac} - v_c = i_{ac}(R_1 + sL_1) \tag{4.12}$$

$$v_c - e_g = i_g[(R_2 + R_g) + s(L_2 + L_g)] \tag{4.13}$$

$$v_c = i_c\left(\frac{1}{sC_f} + R_c\right) \tag{4.14}$$

(a)

(b)
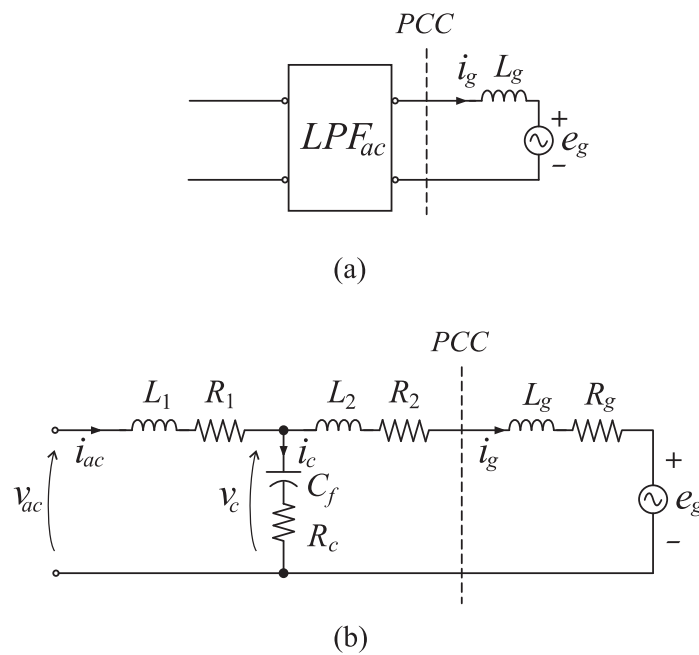
Fig. 4.7. (a) Low pass filter applied in ac micro-grid. (b) LCL-type filter.

Considering (4.10)-(4.13) it is possible to establish the block diagram of the LCL filter as depicted in Fig. 4.8. This block diagram has been employed to design the filter by using bode diagram.
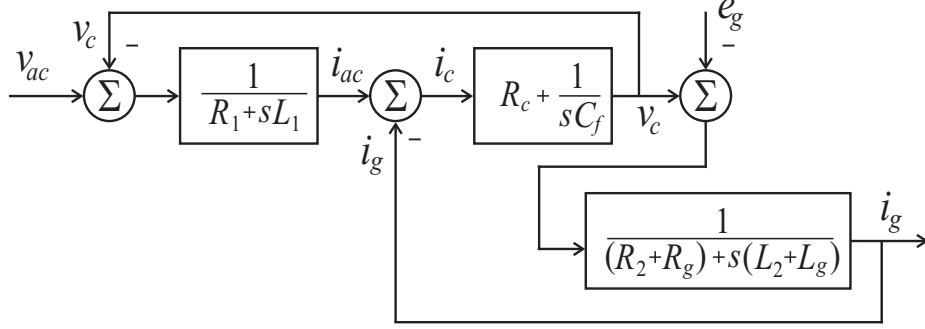
Fig. 4.8. Block diagram of the LCL filter.

4.6 Simulation Results

The parameters employed for the simulation tests were, DG voltage: 200V; $C = 8800uF$; switching frequency: 5kHz; ac link voltage and frequency: $110V$ (RMS) and 60Hz, respectively; and dc link voltage: $45V$.

Fig. 4.9(a) and 4.9(b) show the dc and ac variables for the Mode I (i.e., ac and dc links are demanding energy from the DG) without and with LPF (Low-Pass-Filter), respectively. As expected, with the LPF the voltage applied to the ac link has only its fundamental component.

Fig. 4.10(a) shows the power waveforms for Mode II in which the ac micro-grid has been disconnected after 0.35s. At 0.15s there is a step in the dc reference current meaning more power demanded by the dc microgrid. In this mode only dc micro-grid is demanding energy from DG system. Also Fig. 4.10(b) shows the power waveforms for Mode III, in which the ac micro-grid is the only element demanding energy from the source while dc grid has been disconnected after 0.3s.

Fig. 4.11(a) shows the power waveforms when the ac microgrid is generating instead of demanding power, as it has negative power. In Fig. 4.11(a) the ac power has a negative value and after 0.3s there is a transient in that waveform. At this moment the angle difference between the ac voltage generated by the converter and the voltage of the ac micro-grid has been changed, as discussed in Section V.A.

Fig. 4.11(b) from 0.1s to 0.2s shows the operation of Mode I (both micro-grids are demanding power from DG), while at 0.2s there is a transient in the dc microgrid demanding more power from DG. On the other hand, from 0.3s to 0.45s the dc micro-grid is delivering power to ac microgrid (Mode V); as a consequence, the amount of power delivered from DG is reduced. As expected by the theoretical study, the proposed converter deals with the bidirectional energy power flow required in a hybrid microgrid system.

4.7 Conclusion

In this chapter was studied a power electronics converter able to connect a distributed generation system with a hybrid dc/ac microgrid. Bidirectional power flow capability between dc and ac micro-grids, independent control in both dc and ac parts of the converter, and different operation conditions by using a unique power conversion circuit are the main advantages of the proposed converter.
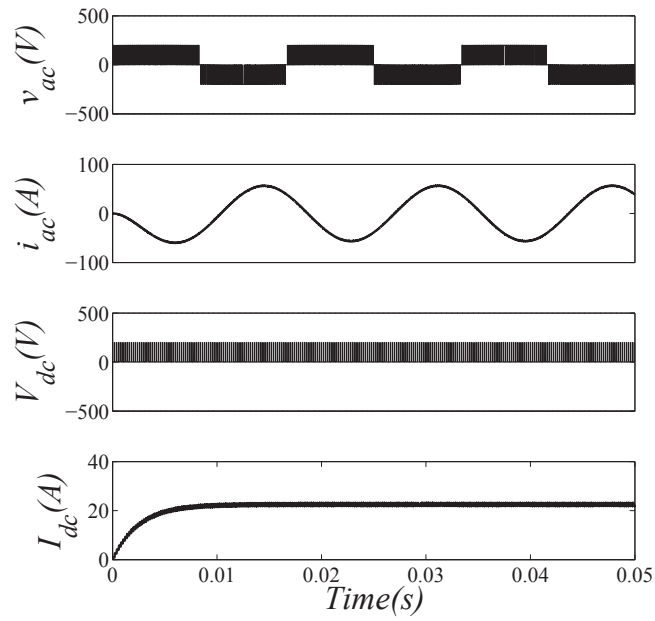
(a)
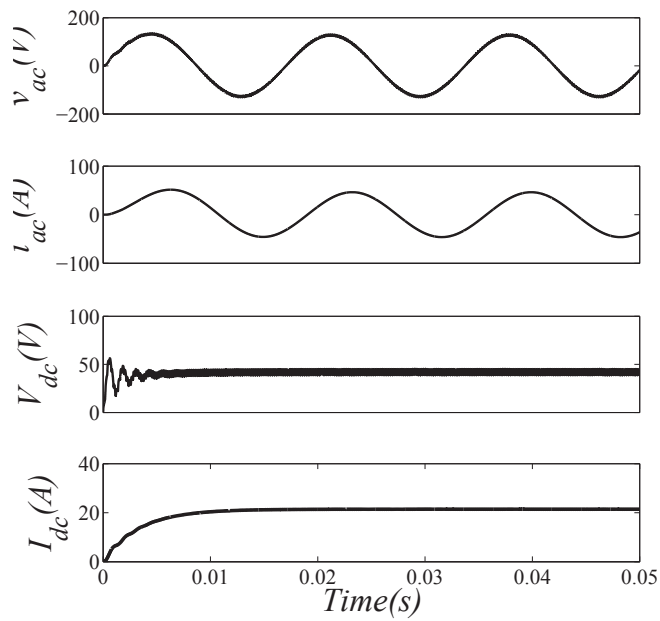
(b)

Fig. 4.9. Results for Mode I (a) without LPF and (b) with LPF, showing (from top to bottom): ac voltage at PCC (v_{ac}), ac output current (i_{ac}), dc output voltage (V_{dc}), and dc output current (I_{dc}).
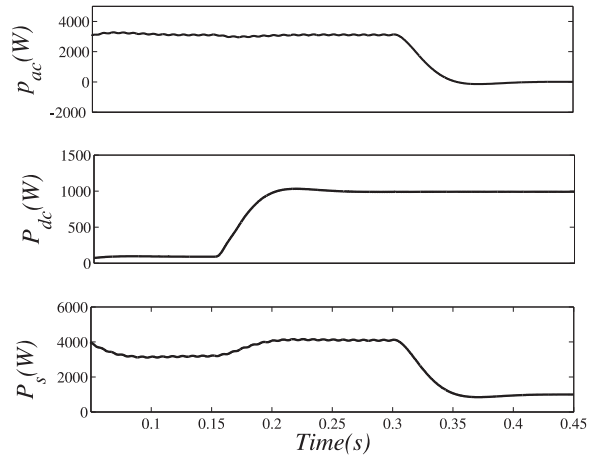
(a)
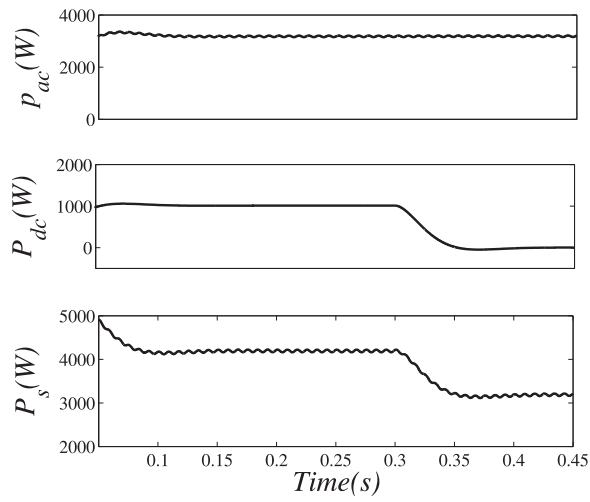
(b)

Fig. 4.10. Simulation results highlighting the power transients and the ability of the proposed converter to handle power flow among different elements in the system.
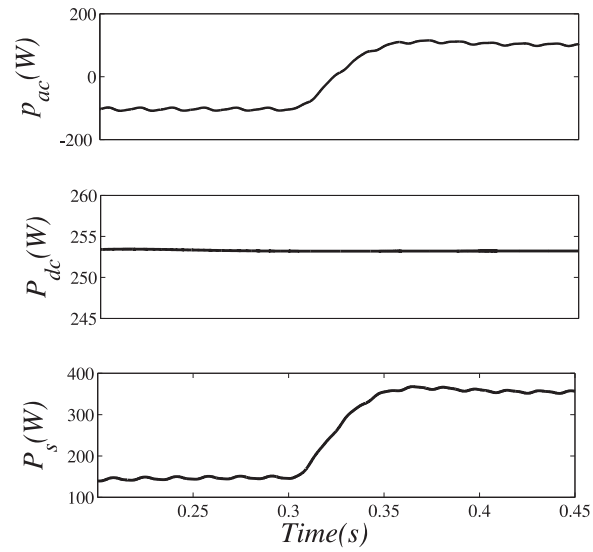
(a)
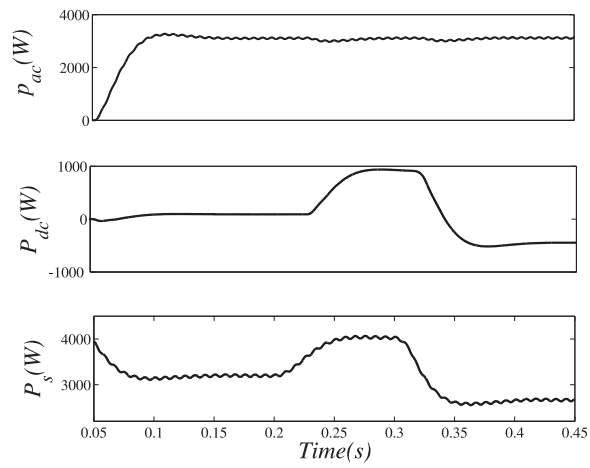
(b)

Fig. 4.11. Simulation results highlighting modes: (a) IV and (b) V.

5. TWO-PHASE MOTOR DRIVE SYSTEM BASED ON A SEVEN-SWITCH CONVERTER

5.1 Introduction

Single-phase machine is popular in applications requiring fractional horse-power motor. For instance, two-phase motors can be found in home appliances, industrial tools or small power applications [75]. It is quite often to employ this type of motor as fixed speed drives, which means that the motor can be connected directly to the utility grid. However, a dc-ac power converter can be used when a variable motor speed operation is required [64], [76].

Symmetrical two-phase motors (with two symmetrical stator circuits shifted by 90 mechanical degrees) can be considered as an interesting alternative for fractional horsepower variable-speed drive, due to its characteristic of no pulsating torque produced as observed in single-phase motors [77]. For instance, the two-phase motor can be used for heating, ventilating, and air-conditioning in hybrid electric vehicles applications [78]. Some hybrid-electrical vehicles have a voltage available at its dc-link connected on the battery stack lower than the required by the inverter [79], [80].

This chapter proposes and studies an integrated converter interfacing a battery with a symmetrical two-phase machine with voltages in quadtrature, as depicted in Fig. 5.1(b). The main advantages of the this converter are reduction of one power switch and high level of integration, while keeping the same features of the conventional solution, such as (i) reduction of one power switch and its drive circuits, and (ii) implementation of two functions using a unique power conversion stage.
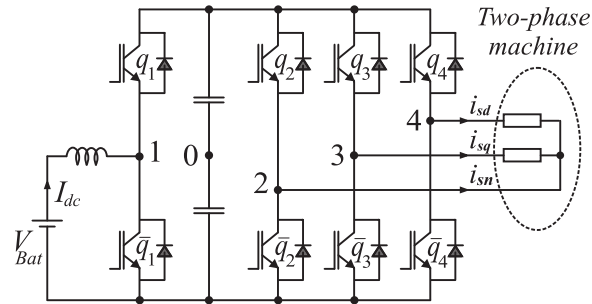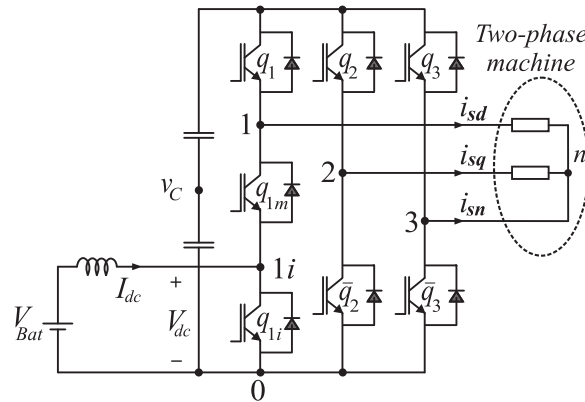
Fig. 5.1. Integrated converter interfacing a two-phase motor drive system: (a) conventional solution with eight switches, and (b) proposed solution with seven switches.

5.2 Converter Model

The proposed converter is shown in Fig. 5.1(b). This converter is composed of seven switches in three legs. The first leg consists of three switches, q_1, q_{1m}, and q_{1i}. The switches in this three-switch leg can not be turned on simultaneously to avoid the short circuit through the dc-link capacitor. Eight switching states are available for this leg that some of them are prohibited. These prohibited states are shown in Table I.

Table 5.1.
Indication of prohibited switching states of three-switch leg.

States	q_1	q_{1m}	q_{1i}	Prohibited States
1	0	0	0	Yes
2	0	0	1	Yes
3	0	1	0	Yes
4	0	1	1	No
5	1	0	0	Yes
6	1	0	1	No
7	1	1	0	No
8	1	1	1	Yes

The equations related to the three-switch leg can be obtained using Table I, as follows:

$$v_{10} = [q_1(1 - q_{1m}q_{1i})]v_c \tag{5.1}$$

$$v_{1i0} = [q_1q_{1m}(1 - q_{1i})]v_c \tag{5.2}$$

Where v_c is the dc-link voltage. In order to define the voltages at ac and dc converter side, it should be necessary to write the equations of the other two legs.

$$v_{20} = q_2v_c \tag{5.3}$$

$$v_{30} = q_3v_c \tag{5.4}$$

where q_2, and q_3 are the state of the switches of the second and third legs.

Once the voltages v_{10}, and v_{20} are defined, it is possible to write the voltages at dc and ac converter sides, i.e.:

$$V_{dc} = v_{1m0} = [q_1q_{1m}(1 - q_{1i})]v_c \tag{5.5}$$

$$v_{sd} = v_{10} - v_{n0} = [q_1(q_{1m} + q_{1i}) - \tag{}$$
$$2q_1q_{1m}q_{1i}]v_c - v_{n0} \tag{5.6}$$

$$v_{sq} = v_{20} - v_{n0} = q_2v_c - v_{n0} \tag{5.7}$$

$$v_{sn} = v_{30} - v_{no} = q_3v_c - v_{n0} \tag{5.8}$$

5.3 PWM Strategy

The gating signals of the switches must be obtained to avoid the prohibited states (short-circuit or one of the unwanted switching states) of the proposed converter as well as to guarantee independent control at both converter sides. If the desired voltages for the dc and ac converter sides are given respectively by V_{dc}^*, v_{sd}^*, and

v_{sq}^* in which $v_{sd}^* = m_a V_s^* \cos(\omega_s t)$, and $v_{sq}^* = m_a V_s^* \cos(\omega_s t + 90^o)$; where m_a is the modulation index, then the reference pole voltages may be expressed as:

$$v_{1i0}^* = V_{dc}^* \tag{5.9}$$

$$v_{10}^* = v_{sd}^* + V_{offset}^* \tag{5.10}$$

$$v_{20}^* = v_{sq}^* + V_{offset}^* \tag{5.11}$$

$$v_{30}^* = V_{offset}^* \tag{5.12}$$

where V_{offset}^* is the voltage to avoid the prohibited states, $(V_{offset}^* = V_{dc}^* + V_s^*)$

This approach to generate the reference pole voltages are presented schematically in Fig. 5.2(a). Fig. 5.2(b) highlights the closed-loop control used to regulate the dc-link capacitor voltage (v_C). The capacitor dc-link voltage v_C is adjusted to a reference value by using PI_v controller. This controller provides the amplitude of the reference current I_{dc}. The current controller is implemented by using a PI controller indicated by PI_i. More details about the PWM and control strategies will be presented in the final version of the paper.

5.4   Control Strategy

Fig. 5.2(b) presents the control block diagram for the proposed converter. The capacitor voltage v_c is adjusted to its reference v_c^* value by using a controller PI_v. This controller provides the amplitude of the reference current I_{dc}^*. The current controller is implemented by using a controller indicated by the block PI_i, which furnishes the voltage V_{dc}^* employed in the PWM scheme presented in Section III. The ac voltages for the three-phase converters have been obtained in open-loop $(v_{sd}^*, v_{sq}^*$ and $v_{sn}^*)$. V_{Bat} in Fig. 5.2(b) is considered as a disturbance for the controller. It is assumed that the current controller will be able to compensate this term.

One way to define the gains of the proportional-integrator (PI) controller is writing the open-loop $[H(s)]$ and closed-loop $[G(s)]$ transfer functions. Assuming that the

(a)

(b)
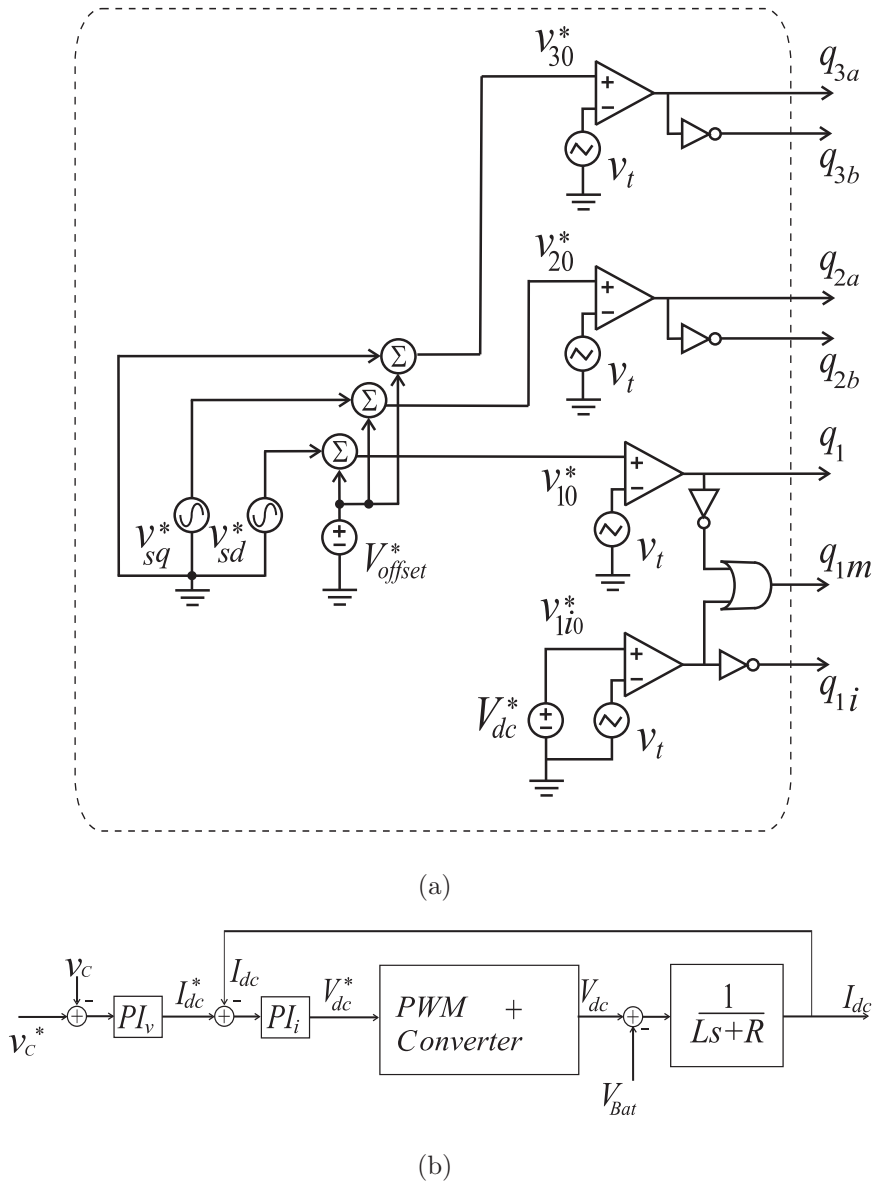
Fig. 5.2. (a) PWM Strategy, and (b) Control Block Diagram.

converter is an ideal controlled voltage source, the open loop transfer function is given by:

$$H(s) = \frac{K_i(\frac{K_p}{K_i}s + 1)}{s} \frac{\frac{1}{R}}{\frac{L}{R}s + 1}. \tag{5.13}$$

Canceling the zero of the controller with the pole of the system, the open loop transfer function depends only of the K_i and R as follows:

$$H(s) = \frac{K_i}{Rs} \tag{5.14}$$

since:

$$\frac{K_p}{K_i} = \frac{L}{R}. \tag{5.15}$$

The closed-loop transfer function is obtained as below:

$$G(s) = \frac{K_i}{K_i + Rs} \tag{5.16}$$

which means a pole placed at:

$$s = \frac{-K_i}{R} \tag{5.17}$$

Equations (13) and (14) are enough to find the controller's gains. The design of the gains of the voltage controller can be obtained similarly.

5.5 DC-Link Capacitor Variables

The dc-link capacitor current (i_{Cap}) for the conventional and proposed converters can be written respectively as following:

$$i_{Cap} = q_1 I_{dc} - q_2 i_{sd} - q_3 i_{sq} - q_4 i_{sn} \tag{5.18}$$

$$i_{Cap} = q_1 (q_{1m} I_{dc} - i_{sd}) - q_2 i_{sq} - q_3 i_{sn}. \tag{5.19}$$

Alternatively, the dc-link capacitor currents for the conventional and proposed converters can be obtained as a function of input and output powers as presented below:

$$i_{Cap} = \frac{P_{in}}{V_{cap}} - \frac{P_{out}}{V_{cap}} \tag{5.20}$$

$$i_{Cap} = \frac{P_{in}}{V_{cap}}(\frac{v_{10}^*}{V_{cap}}) - \frac{P_{out}}{V_{cap}}. \tag{5.21}$$

The power losses on the dc-link capacitor can be calculated by:

$$P_{loss}^{Ho} = 0.45 ESR_{(100Hz)}(I_{c,rms}^{Ho})^2 \tag{5.22}$$

where $ESR_{(100Hz)}$ is the equivalent series resistance at the frequency of 100Hz, and $I_{c,rms}^{Ho}$ is the high-order root mean square (RMS) of the current on the dc-link for high harmonic component ($h > 50$). As ERS is almost constant for frequency higher than 3KHz, the P_{loss}^{Ho} depends only of the $I_{c,rms}^{Ho}$, which means that the reduction of the power losses on the dc-link capacitor is determined by RMS current.

Fig. 5.3 illustrates the harmonic spectrum of the dc-link capacitor current. Comparing (20) with (21) the term v_{10}^*/V_{cap} for the proposed topology will be responsible for the reduction of high frequency components. The proposed topology provides the reduction of the high-order harmonic frequencies when compared with conventional one and consequently the power losses on the capacitor will be lesser.

The dc-link capacitor voltage for the proposed converter is larger than that of the conventional one due to the three-switch leg, which requires a V_{offset} (to avoid the prohibited states). In this case dc-link capacitor voltage is defined by the sum of ac and dc desired voltages.

5.6 Simulated and Preliminary Experimental Results

The system showed in Fig. 1(b) has been simulated using PSIM. The variables used in this simulation are as shown below:

$v_C = 155V; L_i = 2mH; R_o = 10\Omega$ and $L_o = 3mH$.

Fig. 5.4 show the states of the switches at the first leg in Fig. 5.1(b). As it has been discussed above the states of the switches should be in a way to avoid the prohibited states in Table I which depends on the PWM strategy. Fig. 5.4 demonstrates this fact that all the prohibited states are avoided.
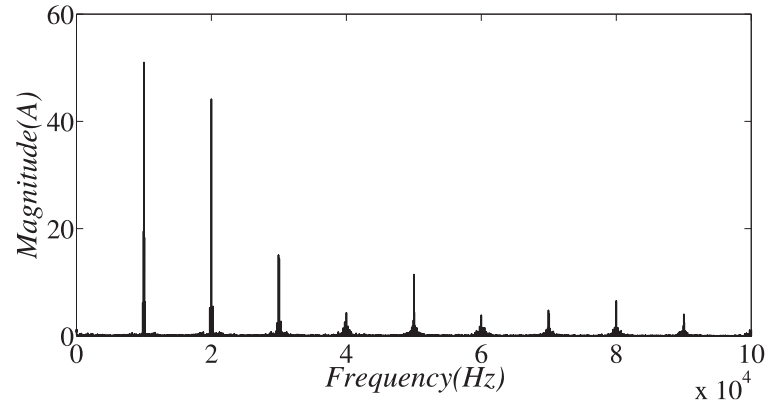
(a)
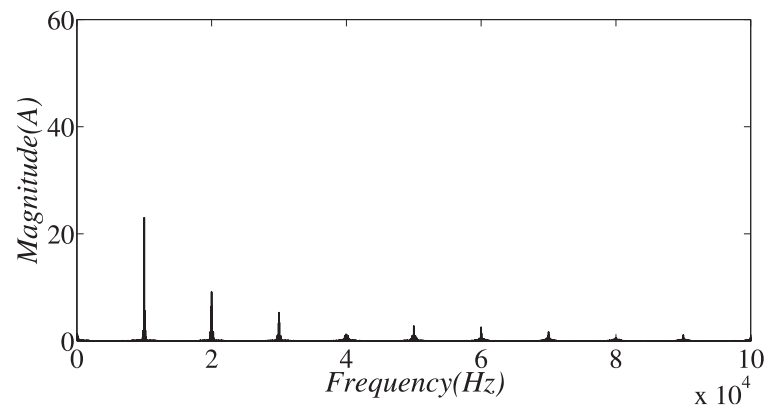
(b)

Fig. 5.3. Spectrum of the dc-link capacitor current: : (a) conventional, and (b) proposed topology.
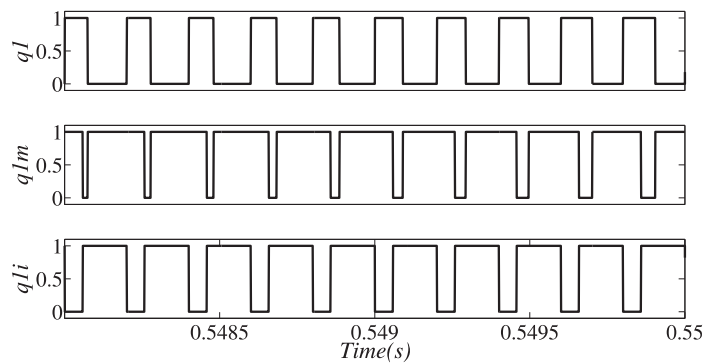
Fig. 5.4. States of the Switches in leg with three switches.

Fig. 5.5 shows the voltages across switches q_1, q_{1m}, and q_{1i}. This figure, as well as Fig. 5.4, demonstrates this fact that the prohibited states are avoided. According to Table I, the states 4,6, and 7 are non prohibited states and Fig. 5.5 shows this fact that the only states available are these three states. The fact of avoiding the prohibited states can also be demonstrated using the currents through switches q_1, q_{1m}, and q_{1i} as depicted in Fig. 5.6.
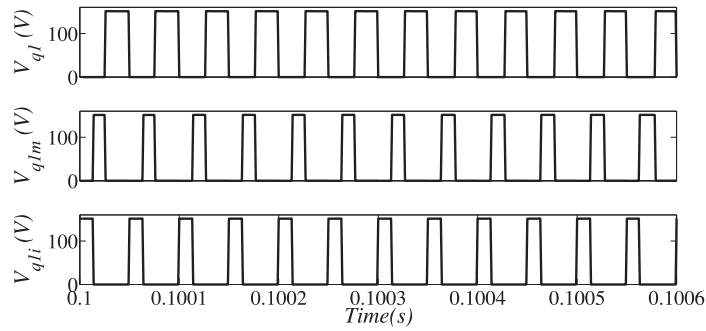
Fig. 5.5. Voltages across switches q_1, q_{1m}, and q_{1i}
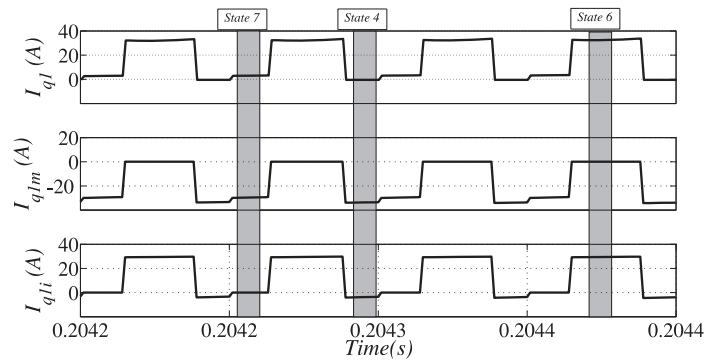
Fig. 5.6. Currents through switches q_1, q_{1m}, and q_{1i}

Fig. 5.7(a) shows the currents for the two-phase motor. As expected, the currents i_{sd} and i_{sq} are in quadrature. Fig. 5.7(b) presents the line to line voltage. Figs. 5.7(c) and 5.7(d) show the operation of the cascade controller. These two figures demonstrate the operation for both controllers. Notice that the measured variables I_{dc} and v_C are following the reference values I_{dc}^* and v_C^*.

5.7 Conclusion

An integrated power electronics solution able to connect a battery with a two-phase machine with bidirectional power flow characteristics is proposed in this paper. The main advantages of this solution are : 1) reduction of one power switch and its drive circuits and 2) implementation of two functions by using a unique power conversion stage. Simulation results were presented in this version of the paper while the experimental results will be presented in the final version of the paper.
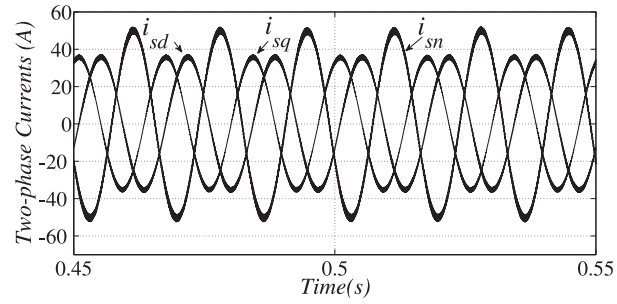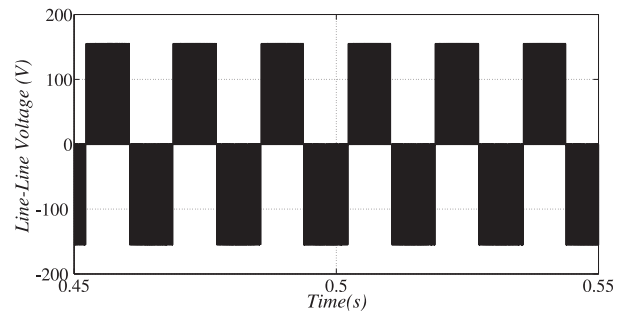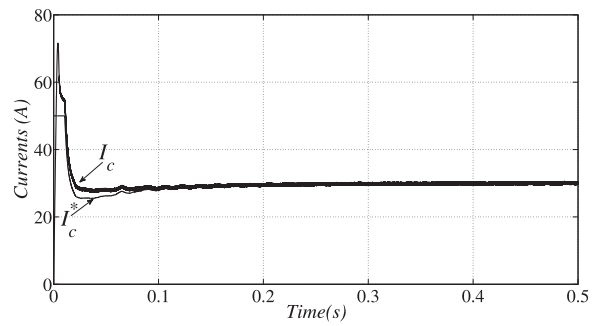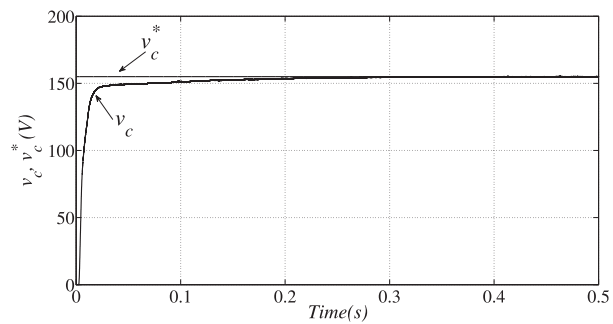
Fig. 5.7. (a) Phase Voltages, (b) Line Voltage at the two-phase machine, (c) Current Controller (PI_i), and (d) Voltage Controller (PI_v).

6. EXPERIMENTAL RESULTS

6.1 Practical Implementation

The experimental results were collected from a dSPACE based system supplying a three-leg inverter operating at 10 kHz. A balanced two-phase load (80 Ω per phase) has been employed for testing the two-phase microgrid under balanced conditions, as presented in Fig. 6.1(a) for a line-to-line voltage equal to 208 V_{RMS}. On the other hand, Fig.6.1(a) presents an unbalanced load with $R_\alpha = 40\Omega$ and $R_\beta = 80\Omega$. Notice that in both cases the inverter guarantees balanced voltage with voltages in quadrature.
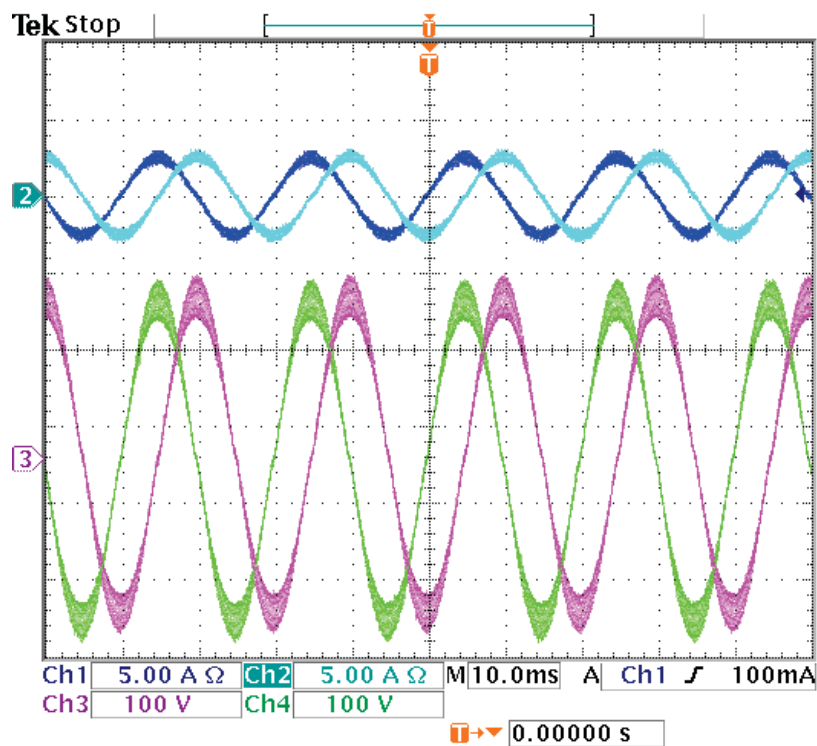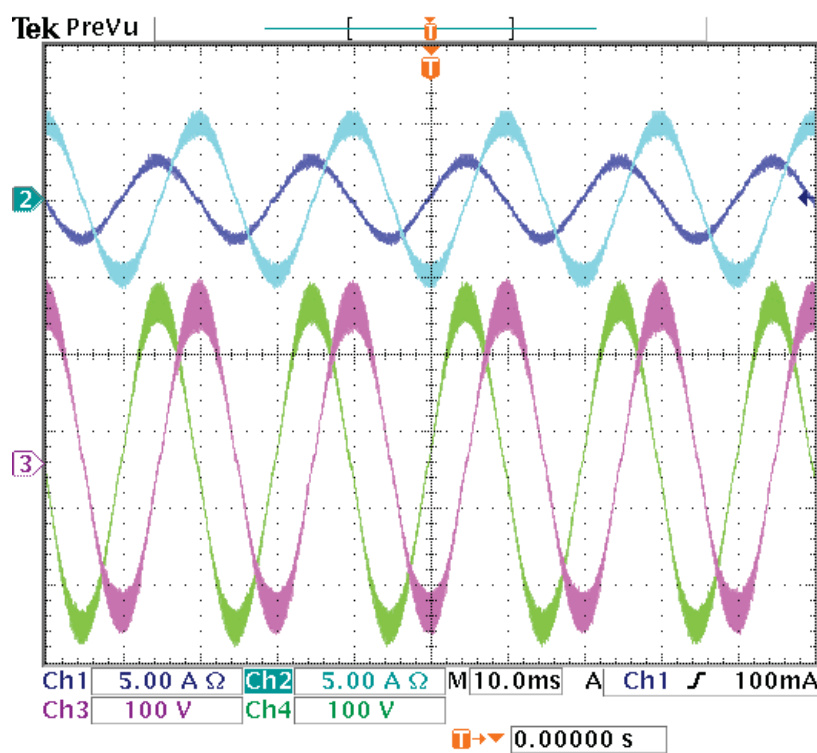
Fig. 6.1. Experimental results for currents (top) and voltages (bottom) waveforms: (a) balanced conditions (b) unbalanced loads. 5 *A/div* and 100 *V/div*.

For testing positive and negative sequences and consequently their ability to represent an unbalanced two-phase system , a set of reference voltages for the PWM has been changed as compared to the tests presented in Fig. 6.1. In this case, the unbalanced condition was created by the reference voltages feeding the PWM module, i.e., positive sequence given by $v_\alpha^{*(+)} = 120cos(2\pi50t+65.83°)$ and $v_\beta^{*(+)} = 120cos(2\pi50t-24.17°)$, while the negative sequence was given by $v_\alpha^{*(-)} = 50cos(2\pi50t + 0.878°)$ and $v_\beta^{*(-)} = 50cos(2\pi50t - 90.878°)$. The results for the symmetrical components are presented in Fig. 6.2.
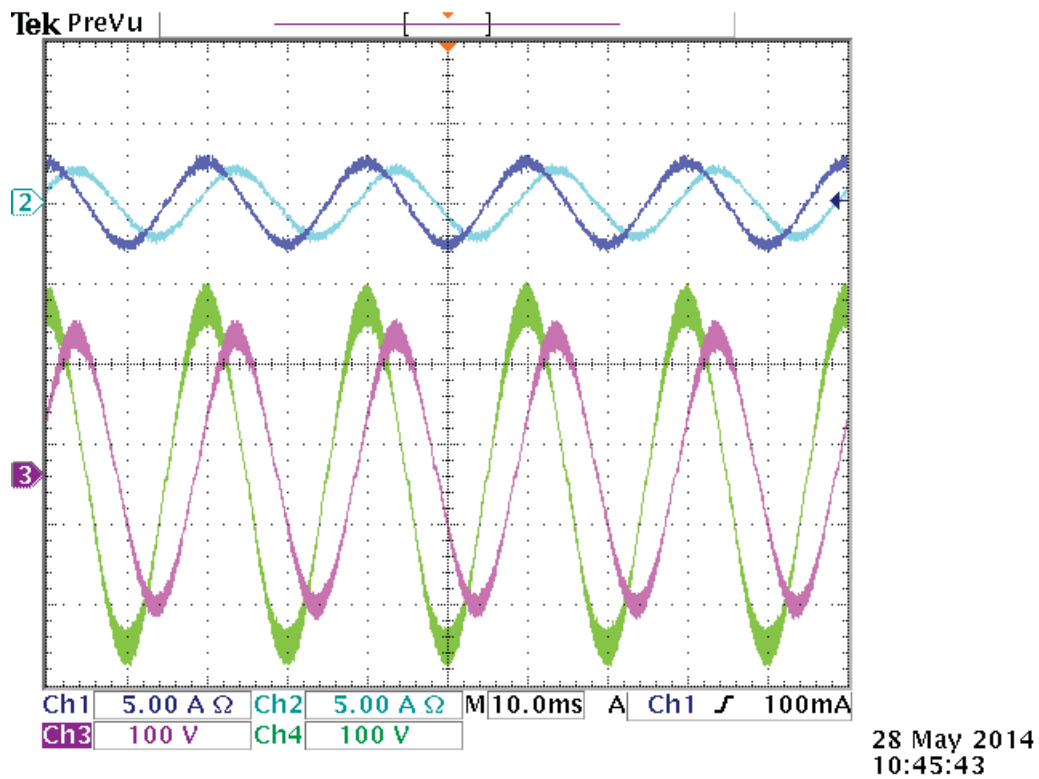
Fig. 6.2. Experimental results with symmetrical components for a two-phase system.

The two-phase microgrid has been also tested with non-linear loads, as presented in Fig. 6.3. Fig. 6.3(a) shows the microgrid voltages in quadrature (bottom waveforms) supplying a non/linear load as presented in Fig. 6.1. In this case the amplitude reference voltages were selected as 100 V_{peak}. Although the presence of the current harmonics, the control system has regulated the voltages satisfactorily. Also, Fig. 6.3(b) shows the results for the same load fed by 200 V_{peak}.
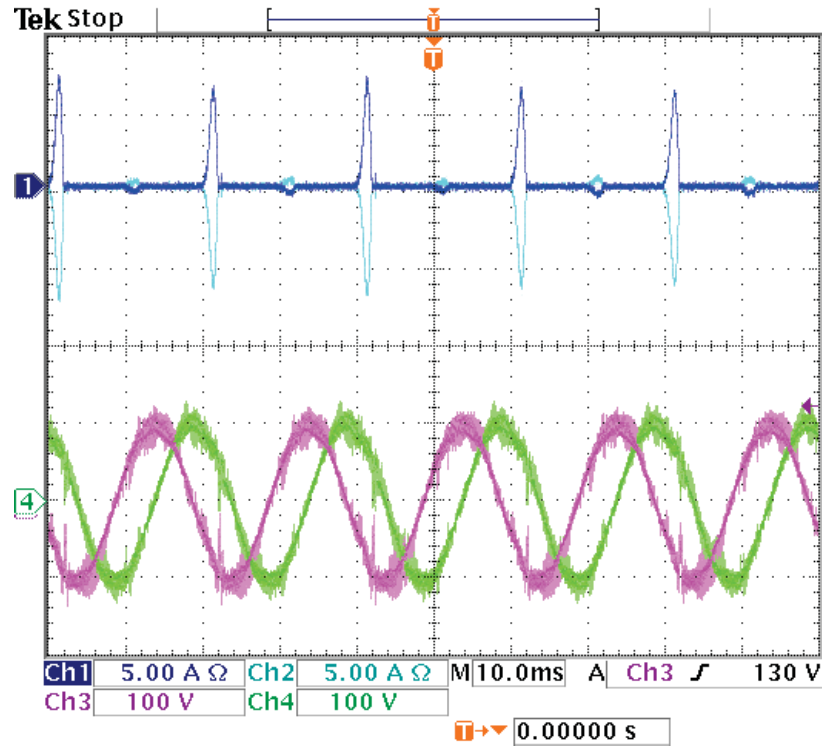
(a)
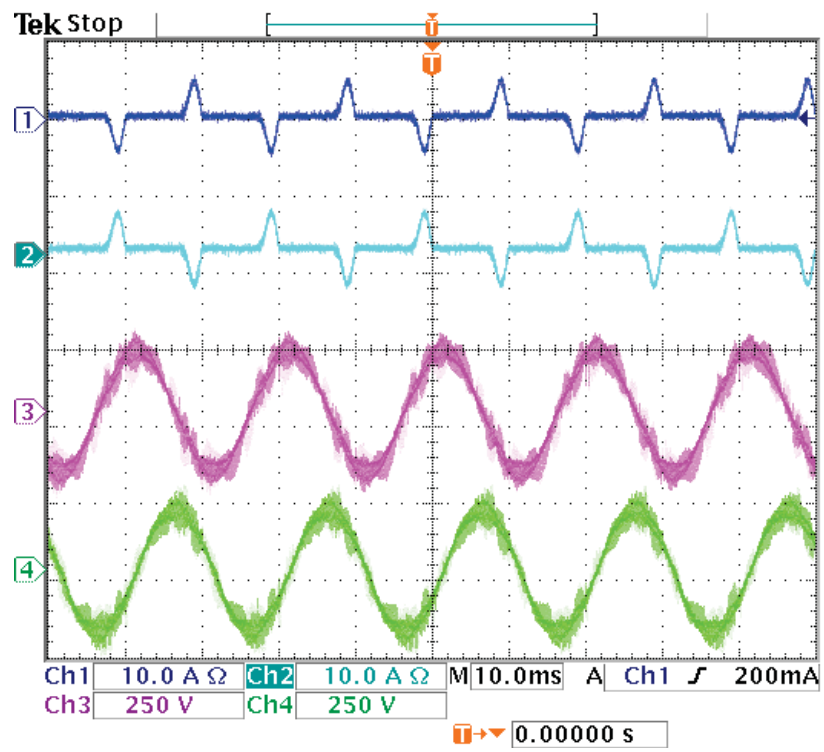
(b)

Fig. 6.3. Experimental results for a two-phase micro-grid supplying a non-linear load with reference voltage equal to: (a) 100 V_{peak}, and (b) 200 V_{peak}.

Fig. 6.4 depicts the currents (top) and voltages (bottom) of the two-phase micro-grid supplying both linear and non-linear loads connected in parallel.
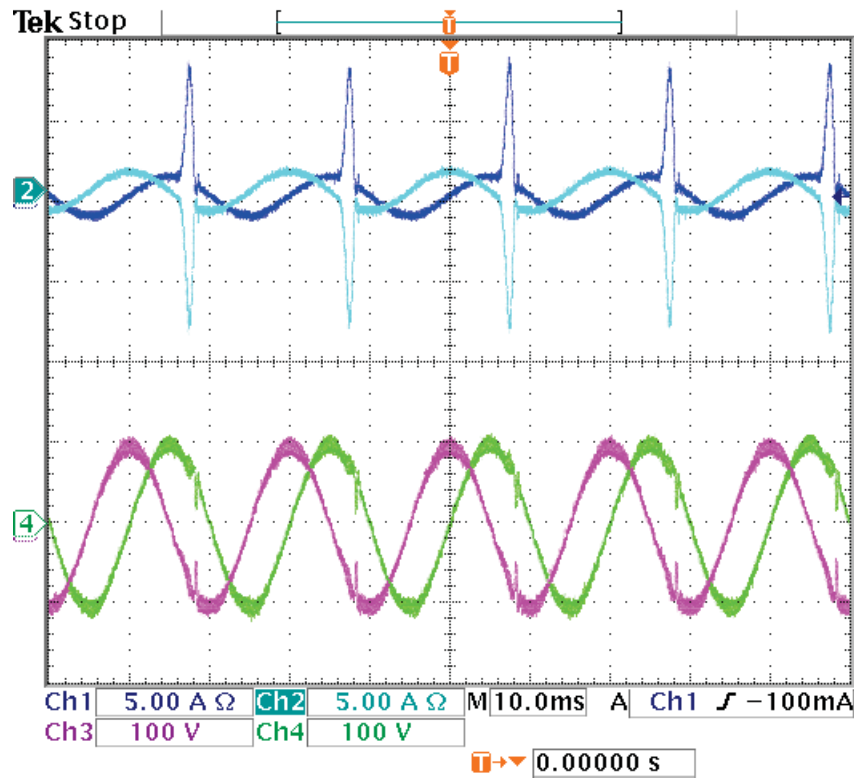
Fig. 6.4. Experimental results for the two-phase system supplying linear and non-linear load.

7. CONCLUSION

This thesis proposed different configurations of power converters such as two leg, five switch power converter and the three leg, seven switch power converter. The main advantage of the new converters is high level of integration with reduction of one power switch, while keeping the same features of the conventional solution, such as (i) bidirectional power flow between dc and ac micro-grids, (ii) independent control in both dc and ac parts, and (iii) different operation conditions using a unique power conversion circuit. Despite proposing a new solution, this chapter presents an analysis of the converter in terms of its operation and PWM strategy, as well as the analysis of the power flow among different elements employed in the system. The proposed five switch converter is interfacing a DG system with a hybrid DC/AC microgrid and there will be independent control on each DC and AC links. This means that whether you have both links available or not, each of these links can be controlled. Also by having DC link available the power can have the bidirectional flow from the DC to the microgrid and vice versa.

Also through this thesis there has been proposed the two-phase microgrid system with voltages in quadrature. The two-phase microgrid consists of three wires, phase α, phase β, and neutral. The main advantage of this microgrid over the three-phase three wire microgrid is that there is two voltages available at this microgrid. Both the line-line voltage (v_{ll}) and the phase voltage (v_{ph}). These two voltages have the relation of $V_{ll} = \sqrt{2}V_{ph}$. The availability of voltages with different amplitudes throughout the line has considerable importance in a microgrid environment.

Finally, the experimental results obtained for the two-phase microgrid validate the theoretical logic and the simulation results obtained during this study.

LIST OF REFERENCES

LIST OF REFERENCES

[1] A. Gonzalez, F. Echavarren, L. Rouco, and T. Gomez, "A sensitivities computation method for reconfiguration of radial networks," *IEEE Transactions on Power Systems*, vol. 27, no. 3, pp. 1294–1301, August 2012.

[2] T.-H. Chen and N.-C. Yang, "Three-phase power-flow by direct zbr method for unbalanced radial distribution systems," *Generation, Transmission Distribution, IET*, vol. 3, no. 10, pp. 903–910, October 2009.

[3] R. Lasseter and P. Paigi, "Microgrid: a conceptual solution," in *Power Electronics Specialists Conference, 2004. PESC 04. 2004 IEEE 35th Annual*, vol. 6, June 2004, pp. 4285–4290.

[4] R. Lasseter, "Microgrids," in *Power Engineering Society Winter Meeting, 2002. IEEE*, vol. 1, 2002, pp. 305–308.

[5] B. Hartono, Y. Budiyanto, and R. Setiabudy, "Review of microgrid technology," in *2013 International Conference on QiR (Quality in Research)*, June 2013, pp. 127–132.

[6] X. Liu, P. Wang, and P. C. Loh, "A hybrid ac/dc micro-grid," in *IPEC, 2010 Conference Proceedings*, October 2010, pp. 746–751.

[7] L. Xiong and W. Peng, "A hybrid ac/dc microgrid and its coordination control," *IEEE Transactions on Smart Grid*, vol. 2, no. 2, pp. 278–286, June 2011.

[8] F. Ding, K. Loparo, and C. Wang, "Modeling and simulation of grid-connected hybrid ac/dc microgrid," in *Power and Energy Society General Meeting, 2012 IEEE*, July 2012, pp. 1–8.

[9] D. Salomonsson, L. Soder, and A. Sannino, "Protection of low-voltage dc microgrids," *IEEE Transactions on Power Delivery*, vol. 24, no. 3, pp. 1045–1053, July 2009.

[10] A. Kahrobaeian and Y.-R. Mohamed, "Interactive distributed generation interface for flexible micro-grid operation in smart distribution systems," *IEEE Transactions on Sustainable Energy*, vol. 3, no. 2, pp. 295–305, April 2012.

[11] C. Wu, J. Liu, and Y. Wu, "The impacts of micro-grid on the reliability of distribution system," in *2012 2nd International Conference on Consumer Electronics, Communications and Networks (CECNet)*, April 2012, pp. 1423–1426.

[12] P. Costa and M. Matos, "Reliability of distribution networks with microgrids," in *Power Tech, 2005 IEEE Russia*, June 2005, pp. 1–7.

[13] I.-S. Bae and J.-O. Kim, "Reliability evaluation of customers in a microgrid," *IEEE Transactions on Power Systems*, vol. 23, no. 3, pp. 1416–1422, August 2008.

[14] A. Basu, S. Chowdhury, and S. P. Chowdhury, "Impact of strategic deployment of chp-based ders on microgrid reliability," *IEEE Transactions on Power Delivery*, vol. 25, no. 3, pp. 1697–1705, July 2010.

[15] J. Kim and H.-I. Park, "Policy directions for the smart grid in korea," *Power and Energy Magazine, IEEE*, vol. 9, no. 1, pp. 40–49, 2011.

[16] H. Liang, B. J. Choi, A. Abdrabou, W. Zhuang, and X. Shen, "Decentralized economic dispatch in microgrids via heterogeneous wireless networks," *IEEE Journal on Selected Areas in Communications*, vol. 30, no. 6, pp. 1061–1074, July 2012.

[17] J. Prajapati, S. Ghadiali, and D. Vora, "Smart grid -a vision for the future," in *2012 International Conference on Advances in Engineering, Science and Management (ICAESM)*, March 2012, pp. 672–677.

[18] R. Lasseter, "Smart distribution: Coupled microgrids," *Proceedings of the IEEE*, vol. 99, no. 6, pp. 1074–1082, June 2011.

[19] H. Nikkhajoei and R. Iravani, "Steady-state model and power flow analysis of electronically-coupled distributed resource units," *IEEE Transactions on Power Delivery*, vol. 22, no. 1, pp. 721–728, January 2007.

[20] M. Hamzeh, H. Karimi, and H. Mokhtari, "A new control strategy for a multibus mv microgrid under unbalanced conditions," *IEEE Transactions on Power Systems*, vol. 27, no. 4, pp. 2225–2232, November 2012.

[21] S. Chakraborty, M. Weiss, and M. Simoes, "Distributed intelligent energy management system for a single-phase high-frequency ac microgrid," *IEEE Transactions on Industrial Electronics*, vol. 54, no. 1, pp. 97–109, February 2007.

[22] Y. W. Li, D. Vilathgamuwa, and P. C. Loh, "A grid-interfacing power quality compensator for three-phase three-wire microgrid applications," *IEEE Transactions on Power Electronics*, vol. 21, no. 4, pp. 1021–1031, July 2006.

[23] Y. Li, D. Vilathgamuwa, and P. C. Loh, "Microgrid power quality enhancement using a three-phase four-wire grid-interfacing compensator," *IEEE Transactions on Industry Applications*, vol. 41, no. 6, pp. 1707–1719, November 2005.

[24] S. Chakraborty and M. Simoes, "Experimental evaluation of active filtering in a single-phase high-frequency ac microgrid," *IEEE Transactions on Energy Conversion*, vol. 24, no. 3, pp. 673–682, September 2009.

[25] W. Peng, L. Xiong, and J. Chi, "A hybrid ac/dc micro-grid architecture, operation and control," in *Power and Energy Society General Meeting, 2011 IEEE*, July 2011, pp. 1–8.

[26] H. Kakigano and Y. Miura, "Dc micro-grid for super high quality distribution 8212; system configuration and control of distributed generations and energy storage devices 8212," in *Power Electronics Specialists Conference, 2006. PESC '06. 37th IEEE*, June 2006, pp. 1–7.

[27] H. Kakigano, Y. Miura, T. Ise, and R. Uchida, "Dc voltage control of the dc micro-grid for super high quality distribution," in *Power Conversion Conference - Nagoya, 2007. PCC '07*, April 2007, pp. 518–525.

[28] B. Patterson, "Dc, come home: Dc microgrids and the birth of the "enernet"," *Power and Energy Magazine, IEEE*, vol. 10, no. 6, pp. 60–69, November 2012.

[29] X. Lu, J. Guerrero, K. Sun, and J. Vasquez, "An improved droop control method for dc microgrids based on low bandwidth communication with dc bus voltage restoration and enhanced current sharing accuracy," *IEEE Transactions on Power Electronics*, vol. 29, no. 4, pp. 1800–1812, April 2014.

[30] J. Guerrero, J. Vasquez, and R. Teodorescu, "Hierarchical control of droop-controlled dc and ac microgrids x2014; a general approach towards standardization," in *Industrial Electronics, 2009. IECON '09. 35th Annual Conference of IEEE*, November 2009, pp. 4305–4310.

[31] A. Khorsandi, M. Ashourloo, and H. Mokhtari, "An adaptive droop control method for low voltage dc microgrids," in *Power Electronics, Drive Systems and Technologies Conference (PEDSTC), 2014 5th*, February 2014, pp. 84–89.

[32] R. Ferreira, H. Braga, A. Ferreira, and P. Barbosa, "Analysis of voltage droop control method for dc microgrids with simulink: Modelling and simulation," in *Industry Applications (INDUSCON), 2012 10th IEEE/IAS International Conference*, November 2012, pp. 1–6.

[33] D. Salomonsson, L. Soder, and A. Sannino, "An adaptive control system for a dc microgrid for data centers," in *Industry Applications Conference, 2007. 42nd IAS Annual Meeting. Conference Record of the 2007 IEEE*, September 2007, pp. 2414–2421.

[34] Y. Ito, Y. Zhongqing, and H. Akagi, "Dc microgrid based distribution power generation system," in *Power Electronics and Motion Control Conference, 2004. IPEMC 2004. The 4th International*, vol. 3, August 2004, pp. 1740–1745.

[35] S. Chakraborty and M. Simoes, "Advanced active filtering in a single phase high frequency ac microgrid," in *Power Electronics Specialists Conference, 2005. PESC '05. IEEE 36th*, June 2005, pp. 191–197.

[36] P. C. Loh, D. Li, Y. K. Chai, and F. Blaabjerg, "Autonomous control of interlinking converter with energy storage in hybrid ac x2013;dc microgrid," *IEEE Transactions on Industry Applications*, vol. 49, no. 3, pp. 1374–1382, May 2013.

[37] E. dos Santos Junior, M. Alibeik, and B. Creek, "New power electronics converter interfacing a dg system with hybrid dc/ac microgrid," in *Power and Energy Conference at Illinois (PECI), 2013 IEEE*, February 2013, pp. 180–185.

[38] F. Katiraei, R. Iravani, N. Hatziargyriou, and A. Dimeas, "Microgrids management," *Power and Energy Magazine, IEEE*, vol. 6, no. 3, pp. 54–65, May 2008.

[39] H. Nikkhajoei and R. Lasseter, "Distributed generation interface to the certs microgrid," *IEEE Transactions on Power Delivery*, vol. 24, no. 3, pp. 1598–1608, July 2009.

[40] M. Akbari, S. M. M. Tafreshi, and M. Golkar, "Voltage control of a hybrid ac/dc microgrid in stand-alone operation mode," in *Innovative Smart Grid Technologies - India (ISGT India), 2011 IEEE PES*, December 2011, pp. 363–367.

[41] J. Zhang, D. Guo, F. Wang, Y. Zuo, and H. Zhang, "Control strategy of interlinking converter in hybrid ac/dc microgrid," in *2013 International Conference onRenewable Energy Research and Applications (ICRERA)*, October 2013, pp. 97–102.

[42] J. Khajesalehi, K. Sheshyekani, M. Hamzeh, and E. Afjei, "A new control strategy for a bidirectional qzsi as an interlink converter in a hybrid ac/dc microgrid," in *Power Electronics, Drive Systems and Technologies Conference (PEDSTC), 2014 5th*, February 2014, pp. 458–463.

[43] N. Eghtedarpour and E. Farjah, "Power control and management in a hybrid ac/dc microgrid," *IEEE Transactions on Smart Grid*, vol. 5, no. 3, pp. 1494–1505, May 2014.

[44] B. Dong, Y. Li, Z. Zheng, and L. Xu, "Control strategies of microgrid with hybrid dc and ac buses," in *Power Electronics and Applications (EPE 2011), Proceedings of the 2011-14th European Conference*, August 2011, pp. 1–8.

[45] Y. W. Li, D. Vilathgamuwa, and P. C. Loh, "A grid-interfacing power quality compensator for three-phase three-wire microgrid applications," *IEEE Transactions on Power Electronics*, vol. 21, no. 4, pp. 1021–1031, July 2006.

[46] F. Tian, K. Siri, and I. Batarseh, "A new single-staged bi-directional high frequency link inverter design," in *Industry Applications Conference, 2006. 41st IAS Annual Meeting. Conference Record of the 2006 IEEE*, vol. 4, October 2006, pp. 1663–1666.

[47] M. Amirabadi, H. Toliyat, and W. Alexander, "A multiport ac link pv inverter with reduced size and weight for stand-alone application," *IEEE Transactions on Industry Applications*, vol. 49, no. 5, pp. 2217–2228, September 2013.

[48] E. dos Santos Junior and M. Alibeik, "Microgrid system with voltages in quadrature," in *Energy Conversion Congress and Exposition (ECCE), 2013 IEEE*, September 2013, pp. 1344–1349.

[49] J. Carrasco, L. Franquelo, J. Bialasiewicz, E. Galvan, R. Guisado, M. Prats, J. Leon, and N. Moreno-Alfonso, "Power-electronic systems for the grid integration of renewable energy sources: A survey," *IEEE Transactions on Industrial Electronics*, vol. 53, no. 4, pp. 1002–1016, June 2006.

[50] N. Mohan, T. M. Undeland, and W. P. Robbins, *Power Electronics Converters, Applications and Design*, 3rd ed. John Wiley and Sons, Inc, 2003.

[51] R. Naik and N. Mohan, "A novel grid interface for photovoltaic, wind-electric, and fuel-cell systems with a controllable power factor of operation," in *Applied Power Electronics Conference and Exposition, 1995. APEC '95. Conference Proceedings 1995., Tenth Annual*, no. 0, March 1995, pp. 995–998.

[52] N. Mohan, "Power electronic circuits: An overview," in *Industrial Electronics Society, 1988. IECON '88. Proceedings., 14 Annual Conference of*, vol. 3, October 1988, pp. 522–527.

[53] A. Maity, A. Patra, N. Yamamura, and J. Knight, "Design of a 20 mhz dc-dc buck converter with 84 percent efficiency for portable applications," in *2011 24th International Conference on VLSI Design (VLSI Design)*, January 2011, pp. 316–321.

[54] F. de Sa, C. Eiterer, D. Ruiz-Caballero, and S. Mussa, "Double quadratic buck converter," in *Power Electronics Conference (COBEP), 2013 Brazilian*, October 2013, pp. 36–43.

[55] M.-X. Lu, B.-H. Hwang, J.-J. Chen, and Y.-S. Hwang, "A sub-1v voltage-mode dc-dc buck converter using pwm control technique," in *2010 IEEE International Conference of Electron Devices and Solid-State Circuits (EDSSC)*, December 2010, pp. 1–4.

[56] J. Wen, T. Jin, and K. Smedley, "A new interleaved isolated boost converter for high power applications," in *Applied Power Electronics Conference and Exposition, 2006. APEC '06. Twenty-First Annual IEEE*, March 2006, p. 6.

[57] K.-B. Park, G.-W. Moon, and M.-J. Youn, "Nonisolated high step-up boost converter integrated with sepic converter," *IEEE Transactions on Power Electronics*, vol. 25, no. 9, pp. 2266–2275, September 2010.

[58] D. Hamill, J. H. B. Deane, and D. Jefferies, "Modeling of chaotic dc-dc converters by iterated nonlinear mappings," *IEEE Transactions on Power Electronics*, vol. 7, no. 1, pp. 25–36, January 1992.

[59] R. P. Severns, G. Bloom, and R. P. Severns, *Modern DC-to-DC switchmode power converter circuits*. Van Nostrand Reinhold Company New York, 1985.

[60] P. Biczel, "Power electronic converters in dc microgrid," in *Compatibility in Power Electronics, 2007. CPE '07*, May 2007, pp. 1–6.

[61] P. Biczel, A. Jasinski, and J. Lachecki, "Power electronic devices in modern power systems," in *EUROCON, 2007. The International Conference on 34;Computer as a Tool 34;*, September 2007, pp. 1586–1586.

[62] T. Blalock, "The first polyphase system: a look back at two-phase power for ac distribution," *Power and Energy Magazine, IEEE*, vol. 2, no. 2, pp. 63–66, March 2004.

[63] L. Stillwell, "The electrical transmission of power from niagara falls," *Amer. Inst. Elect. Engrs*, pp. 444–527, 1901.

[64] F. Blaabjerg, F. Lungeanu, K. Skaug, and M. Tonnes, "Two-phase induction motor drives," *Industry Applications Magazine, IEEE*, vol. 10, no. 4, pp. 24–32, 2004.

[65] J. C. B. Jacobina, E. C. dos Santos and M. B. R. Correa, "Control of the single-phase to three-phase four-leg converter for constant frequency output voltage," in *Proc. IEEE 36th Power Electron. Spec. Conf.*, 2005, pp. 52–58.

[66] C. B. Jacobina, A. M. N. Lima, E. R. C. da Silva, R. N. C. Alves, and P. F. Seixas, "Digital scalar pulse width modulation: a simple approach to introduce non-sinusoidal modulating waveforms," *IEEE Transactions on Power Electron.*, vol. 16, no. 3, pp. 351–359, May 2001.

[67] V. Blasko, "Analysis of a hybrid pwm based on modified space-vector and triangle-comparison methods," *IEEE Transactions on Industrial Applications*, vol. 33, no. 3, pp. 756–764, May/June 1996.

[68] C. B. Jacobina, M. B. R. Correa, T. M. Oliveira, A. M. N. Lima, and E. R. C. da Silva, "Current control of unbalanced electrical systems," in *Conf. Rec. IEEE-IAS Annu. Meeting*, 1999, pp. 1011–1017.

[69] F. Furfari and J. Brittain, "Charles legeyt fortescue and the method of symmetrical components," vol. 8, no. 3, 2002, pp. 7–9.

[70] E. Watanabe, M. Aredes, J. Afonso, J. Pinto, L. Monteiro, and H. Akagi, "Instantaneous p-q power theory for control of compensators in micro-grids," in *Nonsinusoidal Currents and Compensation (ISNCC), 2010 International School*, June 2010, pp. 17–26.

[71] M. Cavalcanti, E. da Silva, D. Boroyevich, W. Dong, and C. Jacobina, "A feasible loss model for igbt in soft-switching inverters," in *Proc. IEEE 34th Power Electron. Spec. Conf.*, 2003, pp. 1845–1850.

[72] A. von Jouanne and B. Banerjee, "Assessment of voltage unbalance," *IEEE Transactions on Power Delivery*, vol. 16, no. 4, pp. 782–790, October 2001.

[73] K. L. Lian and P. Lehn, "Harmonic analysis of single-phase full bridge rectifiers based on fast time domain method," in *Industrial Electronics, 2006 IEEE International Symposium*, vol. 4, July 2006, pp. 2608–2613.

[74] K. L. Lian, B. Perkins, and P. Lehn, "Harmonic analysis of a three-phase diode bridge rectifier based on sampled-data model," *IEEE Transactions on Power Delivery*, vol. 23, no. 2, pp. 1088–1096, April 2008.

[75] N. Abdel-Rahim and A. Shaltout, "An unsymmetrical two-phase induction motor drive with slip-frequency control," *IEEE Transactions on Energy Conversion*, vol. 24, no. 3, pp. 608–616, 2009.

[76] M. Guerreiro, D. Foito, and A. Cordeiro, "A speed controller for a two-winding induction motor based on diametrical inversion," *IEEE Transactions on Industrial Electronics*, vol. 57, no. 1, pp. 449–456, 2010.

[77] M. Jabbar, A. Khambadkone, and Z. Yanfeng, "Space-vector modulation in a two-phase induction motor drive for constant-power operation," *IEEE Transactions on Industrial Electronics*, vol. 51, no. 5, pp. 1081–1088, 2004.

[78] G.-J. Su and J. Hsu, "A five-leg inverter for driving a traction motor and a compressor motor," *IEEE Transactions on Power Electronics*, vol. 21, no. 3, pp. 687–692, 2006.

[79] T. Schoenen, M. Kunter, M. Hennen, and R. De Doncker, "Advantages of a variable dc-link voltage by using a dc-dc converter in hybrid-electric vehicles," in *Vehicle Power and Propulsion Conference (VPPC), IEEE*, September 2010, pp. 1–5.

[80] C. Chan and K. Chau, "An overview of power electronics in electric vehicles," *IEEE Transactions on Industrial Electronics*, vol. 44, no. 1, pp. 3–13, 1997.